

Performance Limits of Single-Anchor mm-Wave Positioning

Anastasios Kakkavas, *Student Member, IEEE*, Mario H. Castañeda Garcia,
Richard A. Stirling-Gallacher, and Josef A. Nossek, *Life Fellow, IEEE*

Abstract

The fundamental limits of single-anchor multi-antenna positioning are investigated. Exploiting the structure of the channel at millimeter-wave (mm-Wave) frequencies, the Cramér-Rao lower bound for the position, orientation and velocity estimation error is derived for transmitter and receiver localization under a static and dynamic scenario with or without knowledge of the time of transmission (KTT). After revisiting the relation of the observed multiple input-multiple output (MIMO)-orthogonal frequency division multiplexing (OFDM) channel with the underlying geometry of the channel, we present geometrically intuitive asymptotic expressions for the Fisher information for large bandwidth, large number of antennas and different levels of KTT. Based on our derived results, we show that the Fisher information matrix (FIM) on position and orientation parameters in the downlink (DL) and the uplink (UL) differ only by a scalar, which is equal to the ratio of the receive Signal-to-Noise Ratio (SNR) in the DL and UL.

Index Terms

mm-Wave, single-anchor positioning, TDOA, TOA, AOD AOA, Doppler shift, Fisher information, Cramér-Rao lower bound, downlink, uplink

I. INTRODUCTION

The 5th generation (5G) of wireless communication networks is on its way, with the vision of providing unprecedentedly high data rates, massive connectivity and reduced latency, among

A. Kakkavas, M. H. Castañeda Garcia and R. A. Stirling-Gallacher are with the Munich Research Center, Huawei Technologies Duesseldorf GmbH, 80992 Munich, Germany (e-mail: {anastasios.kakkavas, mario.castaneda, richard.sg}@huawei.com). A. Kakkavas and J. A. Nossek are with the Department of Electrical and Computer Engineering, Technical University of Munich, 80333 Munich, Germany (e-mail: josef.a.nossek@tum.de). J. A. Nossek is also with the Department of Teleinformatics Engineering, Federal University of Ceara, 60020-180 Fortaleza, Brazil

others, which can be enabled by the large bandwidth available at millimeter-wave (mm-Wave) frequencies, massive number of antennas and dense deployment of base stations. Coincidentally or not, these enablers provide fertile ground for a radical improvement of the positioning capabilities of wireless communication networks [1] and bring localization to the foreground of 5G development. Apart from fusion with Global Navigation Satellite Systems (GNSS) to enhance traditional positioning services, the expected improvement of localization accuracy of communication networks can be a key driving force in the realization of scenarios like assisted living [2], smart factories [3] and automated driving [4], [5], where GNSS and other existing technologies may not be able to guarantee the desired positioning accuracy under all conditions. Moreover, it is anticipated that position information will be used as input to communication-related tasks, such as proactive resource allocation [6], beamforming [7] and beam-alignment [8]. In an effort to unlock the great potential of next generation wireless communication networks, numerous works on the topic have been published. Theoretical analyses for positioning under a multi-anchor setup have been presented in [9]–[13]. Despite promising high accuracy, multi-anchor positioning might be impossible at mm-Wave due to the lack of useful links with more than one anchors. In mm-Wave frequencies the path loss between isotropic antennas¹ is increased, as a consequence of their decreased effective area/aperture, and beamforming gains are required to compensate for it. On the other hand, the fact that more antennas can be packed in the same physical area, allows for multi-antenna transceivers, which enable accurate angle of departure (AOD) and angle of arrival (AOA). Also the large bandwidth available at mm-Wave frequencies enables accurate time of arrival (TOA) or time-difference of arrival (TDOA) measurements. Hence, reliable position estimation is possible with a single anchor.

In recent years, many studies on single-anchor positioning have been published. The single-anchor localization bounds were derived in [14] for arrays with different beamforming strategies, under line-of-sight (LOS)-only propagation, taking synchronization and beamforming weights' quantization errors into account. This work was extended in [15] including multiple input-multiple output (MIMO) transmission and multipath propagation. In [16] the Cramér-Rao lower bound (CRLB) for single-anchor LOS position estimation was presented, deriving a necessary condition on the reference signal for a non-singular Fisher information matrix (FIM). The authors

¹Isotropic antennas are only assumed as a theoretical tool; in practice, antenna elements with potentially similar, but not identical, properties are used.

of [17] provided asymptotic expressions for the position error bounds of systems with large bandwidth and large number of antennas, exploiting the sparsity of the mm-Wave channel, and conducted a comparison between downlink and uplink positioning. In [18] it was shown that the Fisher information provided by single-bounce non-LOS (NLOS) paths is rank-1 and analytic expressions for the direction and intensity of position and orientation information were obtained. In [19], apart from presenting the single-anchor localization error bounds with a multicarrier waveform, an algorithm approaching these bounds for a high signal-to-noise ratio (SNR) was presented. Single-anchor positioning algorithms have also been presented in [20], [21]. Apart from [14], [15], the aforementioned works assume a synchronized system with perfect *knowledge of the time of transmission* (KTT), which is difficult to obtain in a practical communication system. To address this issue, the authors of [22] propose a two-way localization protocol.

In this work we study the performance limits of two-dimensional (2D) single-anchor multi-antenna positioning with a multicarrier waveform² when the both ends of the communication link are static (static scenario) and when the receiver or the transmitter is moving (dynamic scenario), for systems with or without KTT. Following previous works [17]–[19], we consider a sparse mm-Wave channel, where only the single-bounce NLOS paths are strong enough for reception [23]–[26]. With the aim of gaining more insight on the available localization information, we derive the exact FIM and CRLB and then conduct asymptotic analysis of the position, orientation (and velocity) equivalent Fisher information matrix (EFIM) for large bandwidth and number of transmit and receive antennas. The main contributions of this work are the following:

- In the static scenario, using the position and orientation EFIM, additionally to the results presented in [18], [19], we show that the directions of information provided by the single-bounce NLOS paths depend only on the geometry of the channel and not on the system parameters. We study the effect of different levels of KTT on the directions of information from NLOS paths.
- In the dynamic scenario we derive the position, orientation and velocity EFIM, showing the effect of the Doppler shift on the available information. We prove that the information provided by each single-bounce path is rank-3 and provide analytic expressions for the intensity and direction of information.

²The results are also applicable for the SC-FDMA (also known as DFT-s-OFDM) waveform with appropriate design of the reference signal.

- Applying the aforementioned results to the downlink (DL) and the uplink (UL), we show that EFIM on position and orientation parameters in the DL and UL differ only by a scalar, which is equal to the ratio of the receive SNR in the DL and the UL.

The rest of the paper is organized as follows. The system model is derived in Section II. In Section III the Cramér-Rao bound for position and orientation estimation for the static and dynamic scenario is derived. The asymptotic analysis and geometric interpretation of the Fisher information is provided in Section IV. The relation between downlink and uplink positioning is derived in Section V and the effect of KTT is considered in Section VI. Numerical evaluations of the bounds are provided in Section VII and Section VIII concludes the work.

Notation: Throughout this work we use bold lowercase for column vectors, bold uppercase for matrices, non-bold for scalars and calligraphic letters for sets. Depending on its argument, $|\cdot|$ denotes the absolute value of a scalar, the determinant of a matrix or the cardinality of a set. The operators $(\cdot)^T$ and $(\cdot)^H$ denote the transpose and the conjugate transpose of a vector or matrix, $\|\cdot\|_2$ denotes the Euclidean norm of a vector and $\Re\{\cdot\}$ and $\Im\{\cdot\}$ denote the real and imaginary part of a complex number. The i -th element of a vector and the (i, j) -th element of a matrix are denoted by $[\cdot]_i$ and $[\cdot]_{i,j}$, respectively. The i -th row and the j -th column of a matrix are denoted by $[\cdot]_{i,:}$ and $[\cdot]_{:,j}$, respectively. The expectation operator is denoted by $\mathbb{E}[\cdot]$ and, when not otherwise specified, it is applied over the random variables involved in its argument. The set of real and complex numbers are denoted by \mathbb{R} and \mathbb{C} . A multivariate circularly symmetric complex Gaussian distribution with mean $\boldsymbol{\mu}$ and covariance matrix \boldsymbol{C} is denoted by $\mathcal{N}_{\mathbb{C}}(\boldsymbol{\mu}, \boldsymbol{C})$.

II. SYSTEM MODEL

In this section we present the signal model for the static scenario, where both the transmitter and the receiver are static, and, then, we extend the model to the dynamic scenario, where either the transmitter or the receiver is moving.

A. Static Scenario

In Fig. 1 an example of the considered 2D setup is shown. The transmitter and the receiver (Rx) have N_T and N_R antennas and their reference points are at $\boldsymbol{p}_T = [p_{T,x}, p_{T,y}]^T \in \mathbb{R}^2$ and $\boldsymbol{p}_R = [p_{R,x}, p_{R,y}]^T \in \mathbb{R}^2$. Their orientation with respect to (w.r.t.) the horizontal line is α_T and α_R , respectively. The position of the j -th element of the Tx array is given by

$$\boldsymbol{p}_{T,j} = \boldsymbol{p}_T + d_{T,j} \boldsymbol{u}(\psi_{T,j} + \alpha_T) = [p_{T,j,x}, p_{T,j,y}], \quad j = 1, \dots, N_T \in \mathbb{R}^2, \quad (1)$$

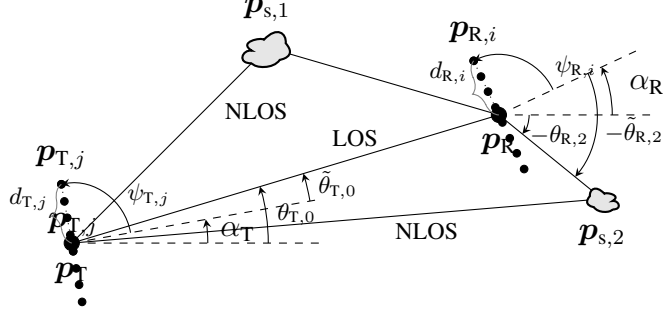


Fig. 1. Geometric model, example with a UCA at the transmitter and a ULA at the receiver.

where $\mathbf{u}(\psi) = [\cos(\psi), \sin(\psi)]^T$ and $d_{T,j}$ and $\psi_{T,j} + \alpha_T$ are its distance and angle from the Tx reference point, as shown in Fig. 1. The quantities for the Rx array are defined accordingly.

We assume that for all antenna pairs there are L discrete propagation paths. The first of these L paths is a LOS ($l = 0$) and the rest are single-bounce paths ($l = 1, \dots, L - 1$). The point of incidence of the l -th single-bounce path, which corresponds either to scattering or reflection, is $\mathbf{p}_{s,l} = [p_{s,l,x}, p_{s,l,y}]^T$, $l = 1, \dots, L - 1$. The array apertures are assumed to be small compared to the distance between Tx and Rx and the distance between each of the scatterers/reflectors and the transmitter and receiver. Therefore, the delay of path l from Tx element j to Rx element i can be approximated by

$$\tau_{l,i,j} \approx \tau_l - \tau_{T,j}(\tilde{\theta}_{T,l}) - \tau_{R,i}(\tilde{\theta}_{R,l}), \quad l = 0, \dots, L - 1, \quad (2)$$

where $\tau_0 = \|\mathbf{p}_R - \mathbf{p}_T\|_2 / c$, $\tau_l = (\|\mathbf{p}_{s,l} - \mathbf{p}_T\|_2 + \|\mathbf{p}_R - \mathbf{p}_{s,l}\|_2) / c$, $l = 1, \dots, L - 1$, with c the speed of light, $\tau_{T,j}(\tilde{\theta}_{T,l}) = d_{T,j} \mathbf{u}^T(\psi_{T,j}) \mathbf{u}(\tilde{\theta}_{T,l}) / c$, and $\tau_{R,i}(\tilde{\theta}_{R,l}) = d_{R,i} \mathbf{u}^T(\psi_{R,i}) \mathbf{u}(\tilde{\theta}_{R,l}) / c$. We assume without loss of generality that $\tau_0 \leq \tau_1 \leq \dots \leq \tau_{L-1}$. The angles are defined as $\tilde{\theta}_{T,l} = \theta_{T,l} - \alpha_T$, $\tilde{\theta}_{R,l} = \theta_{R,l} - \alpha_R$, $l = 0, \dots, L - 1$, where $\theta_{T,0} = \text{atan2}(p_{R,y} - p_{T,y}, p_{R,x} - p_{T,x})$, $\theta_{R,0} = \theta_{T,0} + \pi$, $\theta_{T,l} = \text{atan2}(p_{s,l,y} - p_{T,y}, p_{s,l,x} - p_{T,x}) - \alpha_T$ and $\theta_{R,l} = \text{atan2}(p_{s,l,y} - p_{R,y}, p_{s,l,x} - p_{R,x}) - \alpha_R$, $l = 1, \dots, L - 1$, with $\text{atan2}(y, x)$ being the four-quadrant inverse tangent function.

In the following we provide a detailed derivation of the signal model in order to highlight and facilitate the understanding of the role of parameters related to synchronization and KTT. Assuming high resolution analog-to-digital conversion (ADC) and digital-to-analog conversion (DAC), such that the system is practically linear, the pulse $\tilde{g}(t)$ models all the Tx and Rx processing steps, namely upsampling, digital Tx filtering/pulse shaping, DAC, analog Tx and Rx filtering, ADC, digital Rx filtering/pulse shaping and downsampling. The time support of

$\tilde{g}(t)$ is included in $(0, n_g T_s]$, where n_g is the length of $\tilde{g}(t)$ in integer multiples of the sampling period, T_s is the sampling period and $F_s = 1/T_s$ is the sampling rate. We also assume there is a sampling offset between Tx and Rx, i.e. if an Rx sample starts at time t , a Tx symbol starts at $t + \tau_{\text{off}}$, $0 \leq \tau_{\text{off}} < T_s$. Hence, the discrete-time channel impulse response between Tx antenna j and Rx antenna i is

$$c_{i,j}[m] = \sum_{l=0}^{L-1} h'_l \tilde{g}(mT_s - \tau_{l,i,j} - \tau_{\text{off}}) e^{-j2\pi f_c \tau_{l,i,j}}, \quad (3)$$

where $h'_l \in \mathbb{C}$, $l = 0, \dots, L-1$, are the gains of the propagation paths. We write $\tau_0 + \tau_{\text{off}} = n_0 T_s + \tau_{0,\text{res}}$, $\tau_{L-1} + \tau_{\text{off}} = n_{L-1} T_s + \tau_{L-1,\text{res}}$, $0 \leq \tau_{0,\text{res}}, \tau_{L-1,\text{res}} < T_s$, where we split the path delays into a part which is an integer multiple of the sampling period and a residual. and set n_a as the smallest integer satisfying $n_a T_s > \max_{l,i,j} |\tau_{l,i,j} - n_0 T_s|$, such that the delay between any antenna pair is at most n_a sampling periods larger or smaller than the integer part of the delay between the reference points. Then, the received signal at antenna i for sample n is

$$[\tilde{\mathbf{r}}[n]]_i = \sum_{j=1}^{N_T} \sum_{m=n_0-n_a+1}^{n_{L-1}+n_g+n_a} c_{i,j}[m] [\tilde{\mathbf{x}}[n-m]]_j + [\tilde{\boldsymbol{\eta}}[n]]_i, \quad (4)$$

where $\tilde{\mathbf{x}}[n] \in \mathbb{C}^{N_T}$ is the time-domain transmit signal at sample n and $\tilde{\boldsymbol{\eta}}[n]$ is the zero-mean circularly-symmetric Gaussian noise vector, which is temporally and spatially uncorrelated with variance $2\sigma_{\eta,\text{R}}^2$ per-antenna, i.e. $\tilde{\boldsymbol{\eta}}[n] \sim \mathcal{N}_{\mathbb{C}}(\mathbf{0}, 2\sigma_{\eta,\text{R}}^2 \mathbf{I}_{N_R})$.

We consider a Cyclic Prefix-Orthogonal Frequency Division Multiplexing (CP-OFDM) system with N subcarriers and the CP consisting of N_{CP} samples. N_B OFDM blocks are transmitted and \mathcal{P} is the set indices of the loaded subcarriers. In order to cover systems, where the dimensionality of the digital transmit and receive signals is reduced by hardware constraints, In mm-Wave systems the dimensionality of the digital transmit and receive signals may be reduced by hardware constraints, i.e. the transmitter and the receiver may be equipped with $M_T \leq N_T$ and $M_R \leq N_R$ RF chains, respectively. Therefore, we consider a transmit precoder $\mathbf{P} \in \mathbb{C}^{N_T \times M_T}$ and a receive combiner $\mathbf{W} \in \mathbb{C}^{M_R \times N_R}$ that are applied to all subcarriers. When no precoding (receive combining) is applied $N_T = M_T$ ($N_R = M_R$) and $\mathbf{P} = \mathbf{I}_{N_T}$ ($\mathbf{W} = \mathbf{I}_{N_R}$). The transmit signal vector at subcarrier p , $p \in \mathcal{P}$, of block b , $b = 0, \dots, N_B - 1$, before precoding, is $\mathbf{s}_b[p] \in \mathbb{C}^{M_T}$, and after precoding $\mathbf{x}_b[p] = \mathbf{P} \mathbf{s}_b[p]$. Without loss of generality we assume that the receiver starts collecting samples at time 0. The transmitter starts transmitting the reference signal at time

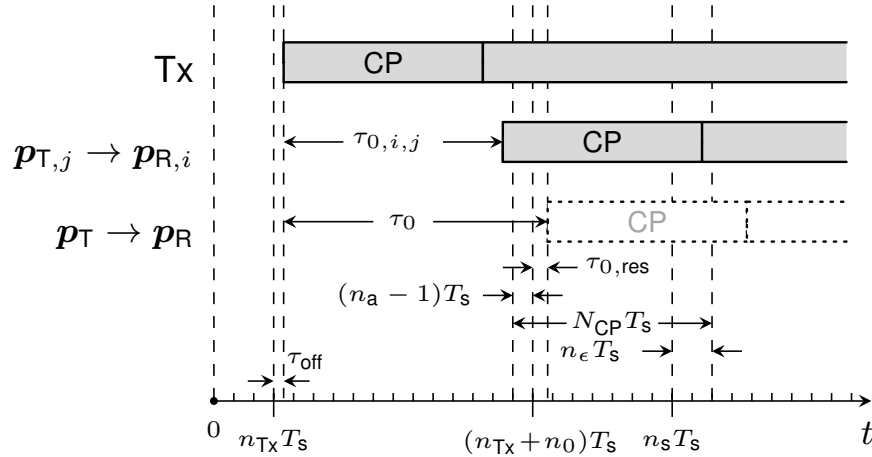


Fig. 2. Timing diagram for the synchronization-related quantities. The relevant timing events are shown for the Tx signal, the signal from the j -th Tx antenna to the i -th Rx antenna and a (hypothetical) signal from the Tx to the Rx reference point.

$n_{TX}T_s + \tau_{off}$, with $n_{TX} \geq 0$ ³. The time-domain transmit signal (after precoding) $\tilde{\mathbf{x}}[n]$ is related to the b -th time-domain OFDM block $\tilde{\mathbf{x}}_b[m]$ as $\tilde{\mathbf{x}}[n_{TX} + bM + m] = \tilde{\mathbf{x}}_b[m]$, where $M = N + N_{CP}$ and $\tilde{\mathbf{x}}_b[m] = \sum_{p \in \mathcal{P}_b} \mathbf{x}_b[p] e^{j \frac{2\pi}{N} p(m - N_{CP})} / \sqrt{N}$, $m = 0 \dots, M - 1$. In order to have access to the reference signal, the receiver needs to synchronize to the transmitter. The coarsely synchronized time-domain received signal $\tilde{\mathbf{y}}[n]$, with synchronization error n_ϵ , is $\tilde{\mathbf{y}}[n] = \tilde{\mathbf{r}}[n + n_s]$, where $n_s = n_{TX} + n_0 - n_a + 1 + N_{CP} - n_\epsilon$. In Fig. 2 we provide a timing diagram depicting all the aforementioned quantities related to the synchronization.

Assuming $N_{CP} \geq n_{L-1} - n_0 + n_g + n_\epsilon + 2n_a$ and $n_\epsilon \geq 0$ to ensure there is no inter-block interference (IBI), we can show that the signal vector at subcarrier p of block b after receive combining is

$$\mathbf{w}_b[p] \approx g[p] e^{-j\omega_p \tau_s} \mathbf{W} \mathbf{A}_R[p] \mathbf{C}[p] \mathbf{A}_T^T[p] \mathbf{x}_b[p] + \mathbf{W} \boldsymbol{\eta}_b[p], \quad (5)$$

where $\omega_p = 2\pi p F_s / N$, $\omega_c = 2\pi f_c$, $\tau_s = (n_\epsilon + n_a - 1)T_s + \tau_{0,res}$, $\mathbf{C}[p] \in \mathbb{C}^{L \times L}$ is a diagonal matrix whose l -th diagonal entry is given by $[\mathbf{C}[p]]_{l,l} = h_l e^{-j\omega_p \Delta \tau_l}$, $h_l = h'_l e^{-j2\pi f_c \tau_l}$, $\Delta \tau_l = \tau_l - \tau_0$, $l = 0, \dots, L - 1$,

$$\begin{aligned} \mathbf{A}_T[p] &= \left[\mathbf{a}_{T,p}(\tilde{\theta}_{T,0}), \dots, \mathbf{a}_{T,p}(\tilde{\theta}_{T,L-1}) \right] \in \mathbb{C}^{N_T \times L}, \\ \mathbf{a}_{T,p}(\tilde{\theta}_{T,l}) &= \left[e^{j(\omega_c + \omega_p)\tau_{T,1}(\tilde{\theta}_{T,l})}, \dots, e^{j(\omega_c + \omega_p)\tau_{T,N_T}(\tilde{\theta}_{T,l})} \right]^T \in \mathbb{C}^{N_T}, \end{aligned}$$

³ n_{TX} could take a certain range of negative values, but that would complicate the illustration without adding to its purpose.

$$\boldsymbol{\eta}_b[p] = \frac{1}{\sqrt{N}} \sum_{m=0}^{N-1} \boldsymbol{\eta}[bM + m + n_s] e^{-j \frac{2\pi}{N} mp}.$$

$\mathbf{A}_R[p]$ is obtained similarly to $\mathbf{A}_T[p]$. The approximate equality in (5) follows from the assumption that, apart from being time-limited, $\tilde{g}(t)$ is *essentially* band-limited⁴. We can interpret τ_s in the following way: if a signal was transmitted from the Tx reference point, τ_s would be the timing offset of its arrival at the Rx reference point from the arrival of the sample which we have synchronized to. We find that

$$\tau_0 = (n_s - N_{CP}) T_s + \tau_s - (n_{TX} T_s + \tau_{\text{off}}). \quad (6)$$

The equation above shows that in order to extract information about the propagation delay of the first path from τ_s , the receiver has to know when the transmitter started sending the reference signal, i.e. it has to have KTT.

B. Dynamic Scenario

We now extend the signal model to the dynamic scenario, with the receiver moving with velocity $\mathbf{v} = [v_x, v_y]^T \in \mathbb{R}^2$. The position of the receiver at time nT_s is $\mathbf{p}_R(nT_s) = \mathbf{p}_{R,0} + \mathbf{v}(n - n_s)T_s$, where $\mathbf{p}_{R,0}$ is its position when the sample we are synchronized to was received, i.e. its position at $t = n_s T_s$. As in the static scenario, we make use of the far field assumption, such that the angles and the channel gains are approximately invariant during the observation interval $N_B M T_s$. The received signal at antenna i is

$$[\tilde{\mathbf{r}}[n]]_i = \sum_{j=1}^{N_T} \sum_{m=n_0-n_a+1}^{n_{L-1}+n_g+n_a} c_{i,j}[m, n] [\tilde{\mathbf{x}}[n-m]]_j + [\tilde{\boldsymbol{\eta}}[n]]_i, \quad (7)$$

where

$$c_{i,j}[m, n] = \sum_{l=0}^{L-1} h'_l \tilde{g} \left(mT_s - \tau_{l,i,j} - \tau_{\text{off}} + \frac{v_l}{c} (n - n_s) T_s \right) e^{-j 2\pi f_c (\tau_{l,i,j} - \frac{v_l}{c} (n - n_s) T_s)}, \quad (8)$$

with $v_l = \mathbf{v}^T \mathbf{u}(\theta_{R,l})$ being the speed of the receiver in the direction of the AOA. We can show that the signal vector at subcarrier p of block b after receive combining is

$$\begin{aligned} \mathbf{w}_b[p] \approx & \sum_{q \in \mathcal{P}} g[q] e^{-j \omega_q \tau_s} \sum_{l=0}^{L-1} h_l e^{-j (\omega_q \Delta \tau_l - \frac{\omega_c + \omega_q}{c} v_l b M T_s)} Q \left(\left(\omega_p - \omega_q - \frac{\omega_c + \omega_q}{c} v_l \right) \frac{T_s}{2} \right) \times \\ & \mathbf{W} \mathbf{a}_{R,q} \left(\tilde{\theta}_{R,l} \right) \mathbf{a}_{T,q}^T \left(\tilde{\theta}_{T,l} \right) \mathbf{x}_b[q] + \mathbf{W} \boldsymbol{\eta}_b[p], \end{aligned} \quad (9)$$

⁴Due to the uncertainty principle, $\tilde{g}(t)$ cannot be both time- and frequency-limited [27].

where $Q(x) = e^{-j(N-1)x} \sin(Nx)/(N \sin(x))$. The Doppler shift $v_l(\omega_c + \omega_q)/c$ is subcarrier-dependent and is an increasing function of the subcarrier index, as expected. Similar to [13], we assume the observation interval is much smaller than the channel coherence time $T_{\text{co}} \propto c/(f_c \|\mathbf{v}\|_2)$ [28]. When the transmitter is moving with velocity \mathbf{v} and the receiver is static, the signal model (9) is still valid with $v_l = \mathbf{v}^T \mathbf{u}(\theta_{T,l})$. The dual mobility case is outside the scope of this work, but can be considered as a straightforward extension.

III. COMPUTATION OF THE CRAMÉR-RAO LOWER BOUND

A. Static Scenario

Based on the received signal model derived in the last section, we will now derive the CRLB for position and orientation estimation for a single-anchor MIMO-OFDM system. Setting $h_{l,\Re} = \Re\{h_l\}$ and $h_{l,\Im} = \Im\{h_l\}$, $l = 0, \dots, L-1$, we define the channel parameter vector ϕ as

$$\begin{aligned} \phi = [\tau_s, \tilde{\theta}_{T,0}, \tilde{\theta}_{R,0}, h_{0,\Re}, h_{0,\Im}, \Delta\tau_1, \tilde{\theta}_{T,1}, \tilde{\theta}_{R,1}, h_{1,\Re}, h_{1,\Im}, \dots, \\ \Delta\tau_{L-1}, \tilde{\theta}_{T,L-1}, \tilde{\theta}_{R,L-1}, h_{L-1,\Re}, h_{L-1,\Im}]^T \in \mathbb{R}^{5L}, \end{aligned} \quad (10)$$

Since ϕ is observed under Gaussian noise, the covariance matrix $\mathbf{C}_{\hat{\phi}}$ of any unbiased estimator $\hat{\phi}$ satisfies [29] $\mathbf{C}_{\hat{\phi}} - \mathbf{J}_{\phi}^{-1} \succeq \mathbf{0}$, where $\succeq \mathbf{0}$ denotes positive semi-definiteness and \mathbf{J}_{ϕ} is the FIM of ϕ . The (i, j) -th entry of the FIM $\mathbf{J}_{\phi} \in \mathbb{R}^{5L \times 5L}$ is

$$[\mathbf{J}_{\phi}]_{i,j} = \frac{1}{\sigma_{\eta,\text{R}}^2} \sum_{b=1}^{N_{\text{B}}} \sum_{p \in \mathcal{P}_b} \Re \left\{ \frac{\partial \mathbf{m}_b^{\text{H}}[p]}{\partial \phi_i} (\mathbf{W} \mathbf{W}^{\text{H}})^{-1} \frac{\partial \mathbf{m}_b[p]}{\partial \phi_j} \right\}, \quad (11)$$

where

$$\mathbf{m}_b[p] = g[p] e^{-j\omega_p \tau_s} \mathbf{W} \mathbf{A}_{\text{R}}[p] \mathbf{C}[p] \mathbf{A}_{\text{T}}^{\text{T}}[p] \mathbf{x}_b[p]. \quad (12)$$

The required derivatives of $\mathbf{m}_b[p]$ are provided in Appendix A.

Instead of ϕ , which includes the unknown channel parameters, we are rather interested in the estimation of a parameter vector including the unknown position parameters. We consider two cases, depending on the available knowledge on the Tx and Rx orientation. In the first case the Tx position \mathbf{p}_{T} and orientation α_{T} are known and the Rx position \mathbf{p}_{R} and orientation α_{R} are unknown. The position parameter vector then reads as

$$\tilde{\phi}_{\text{R}} = [\mathbf{p}_{\text{R}}^{\text{T}}, \alpha_{\text{R}}, \tau_s, h_{0,\Re}, h_{0,\Im}, \mathbf{p}_{\text{s},1}^{\text{T}}, h_{1,\Re}, h_{1,\Im}, \dots, \mathbf{p}_{\text{s},L-1}^{\text{T}}, h_{L-1,\Re}, h_{L-1,\Im}]^T \in \mathbb{R}^{4L+2}. \quad (13)$$

In the second case the Rx estimates the Tx position and orientation, knowing its own position and orientation. The parameter vector is then

$$\tilde{\boldsymbol{\phi}}_{\text{T}} = [\mathbf{p}_{\text{T}}^{\text{T}}, \alpha_{\text{T}}, \tau_{\text{s}}, h_{0,\Re}, h_{0,\Im}, \mathbf{p}_{\text{s},1}^{\text{T}}, h_{1,\Re}, h_{1,\Im}, \dots, \mathbf{p}_{\text{s},L-1}^{\text{T}}, h_{L-1,\Re}, h_{L-1,\Im}]^{\text{T}} \in \mathbb{R}^{4L+2}. \quad (14)$$

An important observation from the signal model (5) is that, unlike $\boldsymbol{\phi}$ which is identifiable for any L , the position parameter vectors $\tilde{\boldsymbol{\phi}}_{\text{R}}$ and $\tilde{\boldsymbol{\phi}}_{\text{T}}$ can be identifiable only if $L \geq 2$. A way to verify this is to consider the LOS-only case ($L = 1$) and express $\mathbf{q} = d_{\text{T,R}} \mathbf{u}(\theta_{\text{T},0})$, where $d_{\text{T,R}} = \|\mathbf{q}\|_2$. Then, there are infinitely many values of $d_{\text{T,R}}$ that would result in the exact same pdf for the observation vector. Hence, without KTT, the LOS path is not sufficient for single-anchor positioning.

The FIMs $\mathbf{J}_{\tilde{\boldsymbol{\phi}}_{\text{R}}}, \mathbf{J}_{\tilde{\boldsymbol{\phi}}_{\text{T}}}$ can be obtained using $\mathbf{J}_{\boldsymbol{\phi}}$ and the transformation matrices $\mathbf{T}_{\text{R}}, \mathbf{T}_{\text{T}} \in \mathbb{C}^{(4L+2) \times 5L}$ [30]:

$$\mathbf{J}_{\tilde{\boldsymbol{\phi}}_{\text{R}}} = \mathbf{T}_{\text{R}} \mathbf{J}_{\boldsymbol{\phi}} \mathbf{T}_{\text{R}}^{\text{T}} \quad (15)$$

$$\mathbf{J}_{\tilde{\boldsymbol{\phi}}_{\text{T}}} = \mathbf{T}_{\text{T}} \mathbf{J}_{\boldsymbol{\phi}} \mathbf{T}_{\text{T}}^{\text{T}}, \quad (16)$$

where $[\mathbf{T}_{\text{R}}]_{i,j} = \partial [\boldsymbol{\phi}]_j / \partial [\tilde{\boldsymbol{\phi}}_{\text{R}}]_i$ and $[\mathbf{T}_{\text{T}}]_{i,j} = \partial [\boldsymbol{\phi}]_j / \partial [\tilde{\boldsymbol{\phi}}_{\text{T}}]_i$. The entries of $\mathbf{T}_{\text{R}}, \mathbf{T}_{\text{T}}$ are given in Appendix B. In the following we will refer to both $\mathbf{J}_{\tilde{\boldsymbol{\phi}}_{\text{R}}}$ and $\mathbf{J}_{\tilde{\boldsymbol{\phi}}_{\text{T}}}$ as $\mathbf{J}_{\tilde{\boldsymbol{\phi}}}$ and to \mathbf{T}_{R} and \mathbf{T}_{T} as \mathbf{T} , explicitly distinguishing between them when necessary.

We use the notion of the equivalent FIM (EFIM) [11], to focus on the available information on the position and orientation parameters. The EFIM can have much lower dimensions than $\mathbf{J}_{\tilde{\boldsymbol{\phi}}}$, but still fully describes the available information on the parameters of interest. Splitting \mathbf{T} as $\mathbf{T} = \begin{bmatrix} \mathbf{T}_{\text{po}}^{\text{T}} & \mathbf{T}_{\text{np}}^{\text{T}} \end{bmatrix}^{\text{T}}$, with \mathbf{T}_{po} consisting of the first three rows of \mathbf{T} corresponding to the position and orientation parameters and \mathbf{T}_{np} the rest, the EFIM for the position and orientation parameters is

$$\mathbf{J}_{\text{po}} = \mathbf{T}_{\text{po}} \mathbf{J}_{\boldsymbol{\phi}} \mathbf{T}_{\text{po}}^{\text{T}} - \mathbf{T}_{\text{po}} \mathbf{J}_{\boldsymbol{\phi}} \mathbf{T}_{\text{np}}^{\text{T}} (\mathbf{T}_{\text{np}} \mathbf{J}_{\boldsymbol{\phi}} \mathbf{T}_{\text{np}}^{\text{T}})^{-1} \mathbf{T}_{\text{np}} \mathbf{J}_{\boldsymbol{\phi}} \mathbf{T}_{\text{po}}^{\text{T}}. \quad (17)$$

The measure we use for characterizing the achievable position estimation accuracy is the position error bound (PEB) defined as [16] $\text{PEB} = \sqrt{[\mathbf{J}_{\text{po}}^{-1}]_{1,1} + [\mathbf{J}_{\text{po}}^{-1}]_{2,2}}$.

B. Dynamic Scenario

In the dynamic scenario the channel parameter vector $\boldsymbol{\phi}$ changes from (10) to

$$\boldsymbol{\phi} = [\tau_{\text{s}}, \tilde{\theta}_{\text{T},0}, \tilde{\theta}_{\text{R},0}, v_0, h_{0,\Re}, h_{0,\Im}, \Delta\tau_1, \tilde{\theta}_{\text{T},1}, \tilde{\theta}_{\text{R},1}, v_1, h_{1,\Re}, h_{1,\Im}, \dots, \Delta\tau_{L-1}, \tilde{\theta}_{\text{T},L-1}, \tilde{\theta}_{\text{R},L-1}, v_{L-1}, h_{L-1,\Re}, h_{L-1,\Im}]^{\text{T}} \in \mathbb{R}^{6L}. \quad (18)$$

When the receiver moves with unknown position, orientation and velocity, the position parameter vector is defined as

$$\tilde{\boldsymbol{\phi}}_{\text{R}} = [\mathbf{p}_{\text{R},0}^{\text{T}}, \alpha_{\text{R}}, \mathbf{v}, \tau_{\text{s}}, h_{0,\mathfrak{R}}, h_{0,\mathfrak{S}}, \mathbf{p}_{\text{s},1}^{\text{T}}, h_{1,\mathfrak{R}}, h_{1,\mathfrak{S}}, \dots, \mathbf{p}_{\text{s},L-1}^{\text{T}}, h_{L-1,\mathfrak{R}}, h_{L-1,\mathfrak{S}}]^{\text{T}} \in \mathbb{R}^{4(L+1)}. \quad (19)$$

The position parameter vector when the transmitter's position, orientation and velocity are unknown can be defined accordingly. We are interested in the EFIM \mathbf{J}_{pov} of the position, orientation and velocity parameters:

$$\mathbf{J}_{\text{pov}} = \mathbf{T}_{\text{pov}} \mathbf{J}_{\phi} \mathbf{T}_{\text{pov}}^{\text{T}} - \mathbf{T}_{\text{pov}} \mathbf{J}_{\phi} \mathbf{T}_{\text{np}}^{\text{T}} (\mathbf{T}_{\text{np}} \mathbf{J}_{\phi} \mathbf{T}_{\text{np}}^{\text{T}})^{-1} \mathbf{T}_{\text{np}} \mathbf{J}_{\phi} \mathbf{T}_{\text{pov}}^{\text{T}}, \quad (20)$$

where we have split $\mathbf{T} \in \mathbb{R}^{4(L+1) \times 6L}$ as $\mathbf{T} = [\mathbf{T}_{\text{pov}}, \mathbf{T}_{\text{np}}]$, with \mathbf{T}_{pov} consisting of the first 5 rows of \mathbf{T} .

IV. ASYMPTOTIC ANALYSIS AND GEOMETRIC INTERPRETATION OF FISHER INFORMATION

The expressions for the FIMs and their entries provided in the last subsection and in Appendix B, although useful for numerical evaluation of the achievable accuracy, do not provide much intuition about the positioning information that is available in the considered single-anchor MIMO-OFDM setup. Our aim is to obtain a geometric interpretation of the Fisher information, as in [13], [18]. Following [17]–[19], we will consider asymptotic expressions for the position and orientation EFIM for large bandwidth⁵ and large number of transmit and receive antennas ($F_{\text{s}}, N_{\text{T}}, N_{\text{R}} \rightarrow \infty$). We will consider arrays whose aperture grows with increasing number of elements, as for arrays with a fixed aperture the asymptotic orthogonality/favorable propagation condition [31], [32] may not be satisfied [33]. In addition to the standard favorable propagation condition $\lim_{N_{\text{T}} \rightarrow \infty} \mathbf{a}_{\text{T},p}^{\text{H}}(\tilde{\boldsymbol{\theta}}_{\text{T},l}) \mathbf{a}_{\text{T},p}(\tilde{\boldsymbol{\theta}}_{\text{T},l'}) / N_{\text{T}} = 0$, we also assume $\lim_{N_{\text{T}} \rightarrow \infty} \frac{\partial}{\partial \tilde{\theta}_{\text{T},l}} \mathbf{a}_{\text{T},p}^{\text{H}}(\tilde{\boldsymbol{\theta}}_{\text{T},l}) \mathbf{a}_{\text{T},p}(\tilde{\boldsymbol{\theta}}_{\text{T},l'}) / N_{\text{T}}^2 = 0$, $\lim_{N_{\text{T}} \rightarrow \infty} \frac{1}{N_{\text{T}}^3} \left\| \frac{\partial}{\partial \tilde{\theta}_{\text{T},l}} \mathbf{a}_{\text{T},p}(\tilde{\boldsymbol{\theta}}_{\text{T},l}) \right\|_2^2 > 0$. Similar assumptions are made for the Rx array. We can verify that these conditions hold for uniform linear arrays (ULAs) and uniform circular arrays (UCAs). In order to focus on the characteristics of the channel and obtain geometrically intuitive expressions for the Fisher information, we also use the following simplifying assumptions:

- 1) As usual in practical implementations, $\tilde{g}(t)$ has a flat frequency response over the occupied subcarriers.

⁵In an OFDM system with a given number of subcarriers and a given set of occupied subcarriers, the occupied bandwidth increases linearly with the sampling rate. Hence, equivalently to writing that the bandwidth goes to infinity we write $F_{\text{s}} \rightarrow \infty$

- 2) $\mathbf{P} = \mathbf{I}_{N_T}$ and $\mathbf{W} = \mathbf{I}_{N_R}$, i.e. the whole transmit and receive spaces (\mathbb{C}^{N_T} and \mathbb{C}^{N_R}) can be sensed.
- 3) The entries of the reference signal $\mathbf{x}_b[p]$ are assumed to be independent and identically distributed (i.i.d) random variables with $\mathbb{E}[\mathbf{x}_b[p]\mathbf{x}_b^H[p]] = \gamma_p P_T/N_T \mathbf{I}_{N_T}$ and $\mathbb{E}[\mathbf{x}_b[p]\mathbf{x}_b^H[q]] = \mathbf{0}$, $p \neq q$. Hence, in this section we compute the entries of the FIMs, taking the expectation over the reference signal, as in [18]:

$$[\mathbf{J}_\phi]_{i,j} = \frac{1}{\sigma_{\eta,R}^2} \sum_{b=1}^{N_B} \sum_{p \in \mathcal{P}_b} \Re \left\{ \mathbb{E} \left[\frac{\partial \mathbf{m}_b^H[p]}{\partial \phi_i} \frac{\partial \mathbf{m}_b[p]}{\partial \phi_j} \right] \right\}. \quad (21)$$

To make the following expressions more compact we set $d_{T,R} = \|\mathbf{p}_R - \mathbf{p}_T\|_2$, $d_{T,s,l} = \|\mathbf{p}_{s,l} - \mathbf{p}_T\|_2$ and $d_{R,s,l} = \|\mathbf{p}_R - \mathbf{p}_{s,l}\|_2$. As before, we distinguish between the static and dynamic scenario.

A. Static Scenario

Before presenting the main results we define a few useful quantities.

Definition 1: The *effective baseband bandwidth* β of the signal is defined as

$$\beta = \sqrt{\sum_{p \in \mathcal{P}} \gamma_p \omega_p^2 - \left(\sum_{p \in \mathcal{P}} \gamma_p \omega_p \right)^2}. \quad (22)$$

Definition 2: The *effective angular carrier frequency* $\bar{\omega}_c$ of the signal is defined as

$$\bar{\omega}_c = \sqrt{\sum_{p \in \mathcal{P}} \gamma_p (\omega_c + \omega_p)^2}. \quad (23)$$

The quantities defined above are the multi-carrier counterparts of the effective baseband bandwidth and the effective carrier frequency defined in [13] for single-carrier systems.

Definition 3: The *squared array aperture function* (SAAF) of the Tx array is defined as [13]

$$S_T(\tilde{\theta}_{T,l}) = \frac{1}{N_T} \sum_{j=1}^{N_T} \left(d_{T,j} \mathbf{u}_\perp(\psi_{T,j}) \mathbf{u}(\tilde{\theta}_{T,l}) \right)^2, \quad (24)$$

where $\mathbf{u}_\perp(\psi) = \mathbf{u}(\psi - \pi/2)$, with the array's centroid chosen as its reference point in our case. The SAAF of the Rx array is defined accordingly. The Tx (Rx) SAAF fully describes the effect of the Tx (Rx) array structure on the AOD (AOA) information.

Theorem 1: Setting $\delta_R = N_R N_B P_T / \sigma_{\eta,R}^2$, the EFIM for the position \mathbf{p}_R and orientation α_R of the receiver when the position and orientation of the transmitter are known and the time of transmission is unknown can asymptotically be expressed as

$$\mathbf{J}_{\text{po}} \rightarrow \delta_R \left(\mathbf{J}_{\text{LOS}} + \sum_{l=1}^{L-1} \mathbf{J}_{\text{NLOS},l} - \mathbf{J}_{\tau_s} \right), \quad (25)$$

where the information from the LOS path is described by

$$\mathbf{J}_{\text{LOS}} = |h_0|^2 \frac{\bar{\omega}_c^2}{c^2 d_{\text{T,R}}^2} \left(S_{\text{T}} \left(\tilde{\theta}_{\text{T},0} \right) \mathbf{z}_{\theta_{\text{T},0}} \mathbf{z}_{\theta_{\text{T},0}}^{\text{T}} + S_{\text{R}} \left(\tilde{\theta}_{\text{R},0} \right) \mathbf{z}_{\theta_{\text{R},0}} \mathbf{z}_{\theta_{\text{R},0}}^{\text{T}} \right), \quad (26)$$

with $\mathbf{z}_{\theta_{\text{T},0}} = \left[\mathbf{u}_{\perp}^{\text{T}}(\theta_{\text{R},0}) \quad 0 \right]^{\text{T}} \in \mathbb{R}^3$ and $\mathbf{z}_{\theta_{\text{R},0}} = \left[\mathbf{u}_{\perp}^{\text{T}}(\theta_{\text{R},0}) \quad -d_{\text{T,R}} \right]^{\text{T}} \in \mathbb{R}^3$, the information from the l -th NLOS path neglecting its coupling with the other paths is described by

$$\mathbf{J}_{\text{NLOS},l} = |h_l|^2 f_l \mathbf{z}_l \mathbf{z}_l^{\text{T}}, \quad (27)$$

with

$$f_l = \frac{1}{\frac{c^2(1+\cos(\Delta\theta_l))^2}{\bar{\omega}_c^2} \left(\frac{d_{\text{T},s,l}^2}{S_{\text{T}}(\tilde{\theta}_{\text{T},l})} + \frac{d_{\text{R},s,l}^2}{S_{\text{R}}(\tilde{\theta}_{\text{R},l})} \right) + \frac{\sin^2(\Delta\theta_l)c^2}{\beta^2}},$$

$$\mathbf{z}_l = \left[\mathbf{u}_{\perp}^{\text{T}}(\theta_{\text{T},l}) + \mathbf{u}_{\perp}^{\text{T}}(\theta_{\text{R},l}) \quad - (1 + \cos(\Delta\theta_l)) d_{\text{R},s,l} \right]^{\text{T}} + \sin(\Delta\theta_l) \left[\mathbf{u}^{\text{T}}(\theta_{\text{R},0}) \quad 0 \right]^{\text{T}} \in \mathbb{R}^3,$$

and the information loss due to coupling among the NLOS paths, induced by the synchronization to the arrival of the LOS path and the unknown time of transmission, is described by

$$\mathbf{J}_{\tau_s} = \frac{1}{K_{\tau_s}} \mathbf{z}_{\tau_s} \mathbf{z}_{\tau_s}^{\text{T}}, \quad (28)$$

where $\mathbf{z}_{\tau_s} = \sum_{l=1}^L |h_l|^2 \sin(\Delta\theta_l) f_l \mathbf{z}_l$, with $K_{\tau_s} = |h_0|^2 \frac{\beta^2}{c^2} + \sum_{l'=1}^{L-1} |h_{l'}|^2 \sin^2(\Delta\theta_{l'}) f_{l'}$.

Proof: See Appendix C. ■

Some interesting remarks are to be made based on the theorem above. Similar to [18], we find that the EFIM of each of the single-bounce NLOS paths is rank-1, but, due to the lack of KTT, the direction of the information is different compared to the one reported in [18]. Leaving aside the effect of the unknown time of transmission, which is accounted for by the 2nd term of \mathbf{z}_l , we can see that the direction of the position information offered by a single-bounce path is determined solely by the geometry and is independent of the system parameters. More specifically, this direction is given by the sum of the 2-D unit vectors pointing to the directions orthogonal to its AOD and AOA.

Similar results can be obtained when the orientation of the transmitter is unknown:

Theorem 2: The EFIM for the position and the orientation of the transmitter when the position and orientation of the receiver are known and the time of transmission is unknown can be asymptotically expressed as in (25), (26), (27) and (28), with $\mathbf{z}_{\theta_{\text{T},0}} = \left[\mathbf{u}_{\perp}^{\text{T}}(\theta_{\text{T},0}) \quad -d_{\text{T,R}} \right]^{\text{T}}$, $\mathbf{z}_{\theta_{\text{R},0}} = \left[\mathbf{u}_{\perp}^{\text{T}}(\theta_{\text{T},0}) \quad 0 \right]^{\text{T}}$, and $\mathbf{z}_l = \left[\mathbf{u}_{\perp}^{\text{T}}(\theta_{\text{T},l}) + \mathbf{u}_{\perp}^{\text{T}}(\theta_{\text{R},l}) - \sin(\Delta\theta_l) \mathbf{u}^{\text{T}}(\theta_{\text{T},0}) \quad - (1 + \cos(\Delta\theta_l)) d_{\text{T},s,l} \right]^{\text{T}}$.

Proof: Similar to the proof of Theorem 1. ■

By observing that $\mathbf{u}_\perp(\theta_{T,0}) = -\mathbf{u}_\perp(\theta_{R,0})$ we see that only the entries of the EFIMs involving the orientation are different; when the orientation of both the transmitter and the receiver is known then the position EFIM is identical in the two cases. It is the uncertainty about the orientation that makes the accuracy of transmitter and receiver positioning different in general. This matches the intuition that in the single-anchor setup the relative position of the nodes is actually estimated and then the known transmitter (receiver) position is added to it to obtain the unknown receiver (transmitter) position. Hence, the only essential difference is that in one case we have to estimate the receiver's orientation, whereas in the other case the transmitter's orientation is to be estimated.

B. Dynamic Scenario

Apart from the assumption made for the static scenario, we additionally assume that $\omega_c \gg \omega_p$, $p \in \mathcal{P}$, namely that the system under consideration is narrowband, in order to keep the expressions relatively simple and gain insight on the effect of the movement of the receiver or the transmitter. Again, before presenting the results, we define a couple of useful quantities.

Definition 4: The *effective baseband bandwidth* of the signal arriving from the l -th path is defined as

$$\beta_l = \sqrt{\frac{\sum_{q \in \mathcal{P}} \xi_{l,q} \gamma_q \omega_q^2}{\xi_l} - \left(\frac{\sum_{q \in \mathcal{P}} \xi_{l,q} \gamma_q \omega_p}{\xi_l} \right)^2}, \quad (29)$$

where $\xi_{l,q} = \sum_{p \in \mathcal{P}} |Q(\Phi_{p,q,l})|^2$ and $\xi_l = \sum_{q \in \mathcal{P}} \gamma_q \xi_{l,q}$ describes the intensity effect of the Doppler shift for the l -th path on the q -th subcarrier, with $\Phi_{p,q,l} = (\omega_p - \omega_q - v_l \omega_c / c) T_s / 2$. Similar to what is reported in [13] for single-carrier systems, the intensity effect is very small and for many practical scenarios can be neglected, i.e. $\xi_{l,q} \approx 1$, l, q . Then, (29) falls back to (22) $\forall l$.

Definition 5: The *root mean square (rms) duration* of the reference signal arriving from the l -th path is

$$t_{\text{rms},l} = T_s \sqrt{\frac{M^2 (N_{\text{B}}^2 - 1)}{12} + n_{\text{B,rms},l}^2}, \quad (30)$$

where

$$n_{\text{B,rms},l}^2 = \frac{\sum_{q \in \mathcal{P}} \gamma_q \sum_{p \in \mathcal{P}} |Q(\Phi_{p,q,l})|^2 (\cot(\Phi_{p,q,l}) - N \cot(N\Phi_{p,q,l}))^2 / 4}{\xi_l} - \left(\frac{\sum_{q \in \mathcal{P}} \gamma_q \sum_{p \in \mathcal{P}} |Q(\Phi_{p,q,l})|^2 (\cot(\Phi_{p,q,l}) - N \cot(N\Phi_{p,q,l})) / 2}{\xi_l} \right)^2. \quad (31)$$

It can be shown that for practical scenarios with $\|\mathbf{v}\|_2/c \ll 1$

$$n_{\text{B,rms},l}^2 \approx n_{\text{B,rms}}^2 = \sum_{q \in \mathcal{P}} \gamma_q \sum_{\substack{p \in \mathcal{P} \\ p \neq q}} \sin^{-2} \left(\frac{\pi}{N} (p - q) \right). \quad (32)$$

We now present the main result for the dynamic scenario:

Theorem 3: The EFIM for the position \mathbf{p}_R , orientation α_R and velocity \mathbf{v} of the receiver when the orientation of the transmitter is known and the time of transmission is unknown can be asymptotically expressed as

$$\mathbf{J}_{\text{pov}} \rightarrow \delta_{R,T} \left(\mathbf{J}_{\text{LOS}} + \sum_{l=1}^{L-1} \mathbf{J}_{\text{NLOS},l} - \mathbf{J}_{\tau_s} \right), \quad (33)$$

where the information from the LOS path is described by

$$\mathbf{J}_{\text{LOS}} = |h_0|^2 \xi_0 \frac{\omega_c^2}{c^2 d_{T,R}^2} \left(S_T \left(\tilde{\theta}_{T,0} \right) \mathbf{z}_{\theta_{T,0}} \mathbf{z}_{\theta_{T,0}}^T + S_R \left(\tilde{\theta}_{R,0} \right) \mathbf{z}_{\theta_{R,0}} \mathbf{z}_{\theta_{R,0}}^T + \rho_0^2 t_{\text{rms},0}^2 \mathbf{z}_{v_0} \mathbf{z}_{v_0}^T \right), \quad (34)$$

where

$$\begin{aligned} \mathbf{z}_{\theta_{T,0}} &= \begin{bmatrix} \mathbf{u}_{\perp}^T(\theta_{R,0}) & 0 & 0 & 0 \end{bmatrix}^T \in \mathbb{R}^5, \\ \mathbf{z}_{\theta_{R,0}} &= \begin{bmatrix} \mathbf{u}_{\perp}^T(\theta_{R,0}) & -d_{T,R} & 0 & 0 \end{bmatrix}^T \in \mathbb{R}^5, \\ \mathbf{z}_{v_0} &= \begin{bmatrix} -\mathbf{u}_{\perp}^T(\theta_{R,0}) & 0 & \frac{d_{T,R}}{\rho_0} \mathbf{u}^T(\theta_{R,0}) \end{bmatrix}^T \in \mathbb{R}^5, \end{aligned}$$

with $\rho_l = \mathbf{v}_l^T \mathbf{u}_{\perp}(\theta_{R,l})$, $l = 0, \dots, L-1$, the information from the l -th NLOS path neglecting its coupling with the other paths is described by

$$\mathbf{J}_{\text{NLOS},l} = |h_l|^2 \xi_l \left(f_{\Delta\tau,\theta,l} \mathbf{z}_{\Delta\tau,\theta,l} \mathbf{z}_{\Delta\tau,\theta,l}^T + f_{\Delta\tau,v,l} \mathbf{z}_{\Delta\tau,v,l} \mathbf{z}_{\Delta\tau,v,l}^T + f_{\theta,v,l} \mathbf{z}_{\theta,v,l} \mathbf{z}_{\theta,v,l}^T \right), \quad (35)$$

with

$$\begin{aligned} f_{\Delta\tau,\theta,l} &= \frac{i_{\Delta\tau_l} i_{\theta_{R,l}} i_{\theta_{T,l}}}{\chi_l}, \quad f_{\Delta\tau,v,l} = \frac{i_{\Delta\tau_l} i_{v_l} i_{\theta_{T,l}}}{\chi_l}, \\ f_{\theta,v,l} &= \frac{i_{\theta_{R,l}} i_{v_l}}{\chi_l} \left(i_{\Delta\tau_l} (1 + \cos(\Delta\theta_l))^2 + i_{\theta_{T,l}} \sin^2(\Delta\theta_l) \right), \\ \chi_l &= (1 + \cos(\Delta\theta_l))^2 i_{\Delta\tau_l} (i_{\theta_{T,l}} + i_{\theta_{R,l}} + i_{v_l}) + \sin^2(\Delta\theta_l) i_{\theta_{T,l}} (i_{\theta_{R,l}} + i_{v_l}), \\ i_{\Delta\tau_l} &= \frac{\beta_l^2}{c^2}, \quad i_{\theta_{T,l}} = \frac{\omega_c^2 S_T \left(\tilde{\theta}_{T,l} \right)}{c^2 d_{T,s,l}^2}, \quad i_{\theta_{R,l}} = \frac{\omega_c^2 S_R \left(\tilde{\theta}_{R,l} \right)}{c^2 d_{R,s,l}^2}, \quad i_{v_l} = \frac{\omega_c^2 \rho_l^2 t_{\text{rms},l}^2}{c^2 d_{R,s,l}^2}, \end{aligned}$$

$$\mathbf{z}_{\Delta\tau,\theta,l} = \begin{bmatrix} \mathbf{u}_{\perp}^T(\theta_{T,l}) + \mathbf{u}_{\perp}^T(\theta_{R,l}) + \sin(\Delta\theta_l) \mathbf{u}^T(\theta_{R,0}) & -(1 + \cos(\Delta\theta_l)) d_{R,s,l} & 0 & 0 \end{bmatrix}^T \in \mathbb{R}^5,$$

$$\mathbf{z}_{\Delta\tau,v,l} = \begin{bmatrix} \mathbf{u}_{\perp}^T(\theta_{T,l}) + \mathbf{u}_{\perp}^T(\theta_{R,l}) + \sin(\Delta\theta_l) \mathbf{u}^T(\theta_{R,0}) & 0 & -(1 + \cos(\Delta\theta_l)) \frac{d_{R,s,l}}{\rho_l} \mathbf{u}^T(\theta_{R,l}) \end{bmatrix}^T \in \mathbb{R}^5,$$

$$\mathbf{z}_{\theta,v,l} = \begin{bmatrix} 0 & 0 & -d_{R,s,l} & \frac{d_{R,s,l}}{\rho_l} \mathbf{u}^T(\theta_{R,l}) \end{bmatrix}^T \in \mathbb{R}^5,$$

and the information loss due to coupling, induced by the synchronization to the arrival of the LOS path and the unknown time of transmission, is described by

$$\mathbf{J}_{\tau_s} = \frac{1}{K_{\tau_s}} \mathbf{z}_{\tau_s} \mathbf{z}_{\tau_s}^T, \quad (36)$$

where

$$\mathbf{z}_{\tau_s} = \sum_{l=1}^L |h_l|^2 \sin(\Delta\theta_l) \xi_l (f_{\Delta\tau,\theta,l} \mathbf{z}_{\Delta\tau,\theta,l} + f_{\Delta\tau,v,l} \mathbf{z}_{\Delta\tau,v,l}),$$

$$K_{\tau_s} = |h_0|^2 \xi_0 \frac{\beta_0^2}{c^2} + \sum_{l'=1}^{L-1} |h_{l'}|^2 \xi_{l'} \sin^2(\Delta\theta_{l'}) (f_{\Delta\tau,\theta,l'} + f_{\Delta\tau,v,l'}).$$

Proof: Similar to the proof of Theorem 1. ■

Some remarks on the theorem above should be made. First, as in the single-carrier case [13], the Doppler shift has a (negligible) effect on the intensity of the Fisher information, accounted for by ξ_l , $l = 0, \dots, L-1$. The Doppler shift of the LOS path offers position information in the direction orthogonal to its AOA, that is angle information. The intuition behind this is that, as an antenna array provides angle information by sampling the space at different locations *simultaneously*, the movement of the receiver also provides angle information by allowing every single antenna element to sample the space at different locations *over time*. The intensity of the position information is proportional to $\rho_0^2 t_{\text{rms},0}^2$. As explained in [13], $\rho_0 t_{\text{rms},0}$ can be interpreted as the *synthetic array aperture* generated by the movement of the receiver for the LOS path.

For the l -th single-bounce NLOS path the synthetic array aperture is $\rho_l t_{\text{rms},l}$. From rank-1 Fisher information in \mathbb{R}^3 in the static scenario, the single-bounce NLOS paths now offer rank-3 information in \mathbb{R}^5 , composed by the three rank-1 matrices determined by $\mathbf{z}_{\Delta\tau,\theta,l}$, $\mathbf{z}_{\Delta\tau,v,l}$ and $\mathbf{z}_{\theta,v,l}$. Only the first two matrices offer position information, in the same direction as in the static scenario. More specifically the first matrix offers position and orientation information and the second matrix position and velocity information. The third rank-1 matrix contains information only about the orientation and the velocity of the receiver. At least one NLOS path, in addition to the LOS path, is required for full rank \mathbf{J}_{pov} . Similar results, which are omitted for brevity, can be obtained in the case with a moving transmitter with unknown orientation and a static receiver.

V. DOWNLINK VS UPLINK POSITIONING

Assume the DL of a communication system, where the base station (BS) with known orientation is the transmitter and the user equipment (UE), whose orientation is assumed to be

TABLE I
MAPPING OF THEOREM 1 AND 2 TO DL AND UL POSITIONING.

	BS: Known position and orientation	UE: Unknown position and orientation	
DL	Tx	————→	Rx
UL	Rx	←————	Tx
			Theorem 1
			Theorem 2

unknown, is the receiver. Using (25) or (33) and replacing the subscript 'T' with 'BS' and the subscript 'R' with 'UE', we get the following expression for the DL position and orientation EFIM

$$\mathbf{J}_{\text{po,DL}} \rightarrow \delta_{\text{UE,BS}} \left(\mathbf{J}_{\text{LOS}} + \sum_{l=1}^{L-1} \mathbf{J}_{\text{NLOS},l} - \mathbf{J}_{\tau_s} \right), \quad (37)$$

where \mathbf{J}_{LOS} , $\mathbf{J}_{\text{NLOS},l}$ and \mathbf{J}_{τ_s} are obtained from (26)-(28) in the static or (34)-(36) in the dynamic scenario by replacing the subscripts 'T' and 'R' as described above.

In the UL of a communication system the base station (BS) is the receiver and the user equipment (UE) is the transmitter. Using the expressions for the position and transmitter orientation EFIM and replacing the subscript 'R' with 'BS' and the subscript 'T' with 'UE', we get the following expression for the UL positioning EFIM

$$\mathbf{J}_{\text{po,UL}} \rightarrow \frac{\delta_{\text{BS,UE}}}{\delta_{\text{UE,BS}}} \mathbf{J}_{\text{po,DL}} = \frac{\sigma_{\eta,\text{UE}}^2 N_{\text{BS}} P_{\text{UE}}}{\sigma_{\eta,\text{BS}}^2 N_{\text{UE}} P_{\text{BS}}} \mathbf{J}_{\text{po,DL}}. \quad (38)$$

Table I depicts how Theorems 1 and 2 are mapped to the DL and UL scenarios.

From (38) we see that DL and UL positioning have in general different accuracy, owing to different receive SNR. Under the same receive SNR, there is DL and UL positioning duality. Compared to the DL, in the UL we can benefit from the higher number of antennas of the BS and the typically better noise figures, but on the other hand we typically have a much lower power budget at the UE. Furthermore, in our expressions we can see that the arrays' orientation influences the CRLB only through the SAAFs and affects the DL and the UL in the same way.

VI. POSITIONING WITH KNOWLEDGE OF THE TIME OF TRANSMISSION

In this section we show how the KTT changes the Fisher information for position and orientation estimation. We focus here on static scenario and the case where \mathbf{p}_R and α_R are unknown. The analysis for the dynamic scenario or the case where \mathbf{p}_T and α_T are unknown is very similar and we omit it for brevity.

Let us assume that the receiver has (imperfect) KTT, namely it works under the premise that the signal was transmitted at $n_{\text{Tx}}T_s + \tau_{\text{off}} + \epsilon_{\text{clk}}$, where ϵ_{clk} is the clock synchronization error, which we assume to be a zero-mean Gaussian distributed random variable with variance σ_{clk}^2 . Then the receiver can compute

$$\begin{aligned}\hat{\mathbf{w}}_b[p] &= \mathbf{w}_b[p]e^{-j\omega_p((n_s - N_{\text{CP}} + n_{\text{Tx}})T_s + \tau_{\text{off}} + \epsilon_{\text{clk}})} \\ &= g[p]e^{-j\omega_p\epsilon_{\text{clk}}}\mathbf{W}\mathbf{A}_R[p]\hat{\mathbf{C}}[p]\mathbf{A}_T^T[p]\mathbf{x}_b[p] + \mathbf{W}\boldsymbol{\eta}_b[p],\end{aligned}\quad (39)$$

where $\mathbf{C}[p] \in \mathbb{C}^{L \times L}$ is now a diagonal matrix whose $(l+1)$ -th diagonal entry is given by $[\mathbf{C}[p]]_{l+1,l+1} = h_l e^{-j\omega_p\tau_l}$, $l = 0, \dots, L-1$. In this case we compute the Bayesian CRLB, that is we average the CRLB for a given realization of ϵ_{clk} over its distribution. With similar steps to the sections above we can show that the position and orientation EFIM is

$$\mathbf{J}_{\text{po}}^{(\text{KTT})} = \delta_{\text{R,T}} \left(\mathbf{J}_{\text{LOS}}^{(\text{KTT})} + \sum_{l=1}^{L-1} \mathbf{J}_{\text{NLOS},l}^{(\text{KTT})} - \mathbf{z}^{(\text{KTT})} (\mathbf{z}^{(\text{KTT})})^T / K^{(\text{KTT})} \right), \quad (40)$$

where

$$\begin{aligned}\mathbf{J}_{\text{LOS}}^{(\text{KTT})} &= |h_0|^2 \frac{\beta^2}{c^2} \mathbf{z}_{\tau_0} \mathbf{z}_{\tau_0}^T + |h_0|^2 \frac{\bar{\omega}_c^2}{c^2 d_{\text{T,R}}^2} \left(S_{\text{T}}(\tilde{\theta}_{\text{T},0}) \mathbf{z}_{\theta_{\text{T},0}} \mathbf{z}_{\theta_{\text{T},0}}^T + S_{\text{R}}(\tilde{\theta}_{\text{R},0}) \mathbf{z}_{\theta_{\text{R},0}} \mathbf{z}_{\theta_{\text{R},0}}^T \right), \\ \mathbf{J}_{\text{NLOS},l}^{(\text{KTT})} &= |h_l|^2 f_l \mathbf{z}_l^{(\text{KTT})} (\mathbf{z}_l^{(\text{KTT})})^T, \\ \mathbf{z}_{\tau_0} &= \left[-\mathbf{u}^T(\theta_{\text{R},0}) \quad 0 \right]^T, \\ \mathbf{z}_l^{(\text{KTT})} &= \left[\mathbf{u}_{\perp}^T(\theta_{\text{T},l}) + \mathbf{u}_{\perp}^T(\theta_{\text{R},l}) \quad -(1 + \cos(\Delta\theta_l)) d_{\text{R},s,l} \right]^T, \\ \mathbf{z}^{(\text{KTT})} &= |h_0|^2 \beta^2 / c^2 \mathbf{z}_{\tau_0} + \sum_{l=1}^{L-1} |h_l|^2 \sin(\Delta\theta_l) f_l \mathbf{z}_l^{(\text{PK})}, \\ K^{(\text{KTT})} &= 1 / (\delta_{\text{R,T}} \sigma_{\text{clk}}^2) + |h_0|^2 \frac{\beta^2}{c^2} + \sum_{l'=1}^{L-1} |h_{l'}|^2 \sin^2(\Delta\theta_{l'}) f_{l'}.\end{aligned}$$

We note that $\sigma_{\text{clk}}^2 \rightarrow 0$ implies perfect KTT/clock synchronization and in this case (40) is in agreement with [18], but we can now clearly see that the direction of the information from the NLOS path depends only on the geometry, i.e. the positions of the transmitter, receiver and scatterer. For $\sigma_{\text{clk}}^2 \rightarrow \infty$ (40) converges to (25).

VII. NUMERICAL RESULTS

In this section we numerically evaluate the expressions derived above. For the channel model, we follow [18]: the magnitude of the coefficient of the LOS path is $|h_0| = \lambda_c / (4\pi d_{\text{T,R}})$,

the magnitude of the NLOS paths, which are assumed to come from reflections, is $|h_l| = \Gamma_{\text{refl}}\lambda_c/(4\pi(d_{\text{T},s,l} + d_{\text{R},s,l}))$, with the reflection coefficient $\Gamma_{\text{refl}} = 0.1$ and the phase of all the paths is uniformly distributed.

A. Accuracy of the asymptotic expressions

In Fig. 3 we evaluate the accuracy of the asymptotic expressions derived in Sec. IV for the FIM and, consequently, for the position and orientation CRLB, comparing them with the exact expressions from Sec. III. Referring to the exact PEB as PEB_{ex} and to the asymptotic PEB as PEB_{as} , we define the relative error ε_{as} of the asymptotic expressions as $\varepsilon_{\text{as}} = (\text{PEB}_{\text{as}} - \text{PEB}_{\text{ex}}) / \text{PEB}_{\text{ex}}$. We consider a setup where the transmitter and the receiver are equipped with UCAs with $\lambda_c/2$ -spaced elements, where $\lambda_c = c/f_c$ with $f_c = 38$ GHz. The orientation of the arrays is irrelevant as the SAAF of a UCA independent of the angle. The transmitter's reference point is located at the origin, i.e. $\mathbf{p}_{\text{T}} = [0, 0]^{\text{T}}$ and the receiver and two reflectors are randomly placed in a circle of 50 m radius with the following two restrictions: i) the receiver is in the far field of the transmitter and the reflectors are in the far field of the transmitter and the receiver, i.e. $d_{\text{T},\text{R}}, \{d_{\text{T},s,l}, d_{\text{R},s,l}\}_{l=1}^{L-1} > d_f$, where $d_f = 2D^2/\lambda$ is the Fraunhofer distance, with D being the largest dimension of the array; ii) the angular separation of the resulting propagation paths both at the transmitter and the receiver is at least 3° . The sampling frequency is set to $F_s = 245.76$ MHz and the DFT size is $N = 1024$, resulting in a subcarrier spacing of 240 kHz. The set of loaded subcarriers is $\mathcal{P} = \{-297, -291, \dots, 291, 297\}$ and $\gamma_p = 1/|\mathcal{P}|$, $\forall p \in \mathcal{P}$, with $|\mathcal{P}| = 100$. The power per subcarrier is 0 dBm, thus $P_{\text{T}} = 20$ dBm. The noise spectral density is $N_0 = -170$ dBm. We plot ε_{as} as a function of the number of N_{T} and N_{R} , averaging over 5000 random geometry realizations. In order to satisfy the far field assumption and simultaneously keep the geometry fixed with varying number of antennas, we require that $d_{\text{T},\text{R}}, \{d_{\text{T},s,l}, d_{\text{R},s,l}\}_{l=1}^{L-1} > 0.41$ m, which is the Fraunhofer distance for a UCA with 32 elements. We can see that, for both minimum angular separations, the asymptotic expressions are a good approximation of the exact bounds, even for a moderate number of antennas. Also, the smaller the minimum angular separation is, the more antennas are required for the asymptotic bounds to approach the exact bounds.

B. The importance of the knowledge of the time of transmission

We now compare systems with or without KTT. We set $N_{\text{T}} = N_{\text{R}} = 32$ and keep the other system parameters fixed. We also fix the position of the transmitter at $\mathbf{p}_{\text{T}} = [0 \text{ m}, 0 \text{ m}]^{\text{T}}$, the

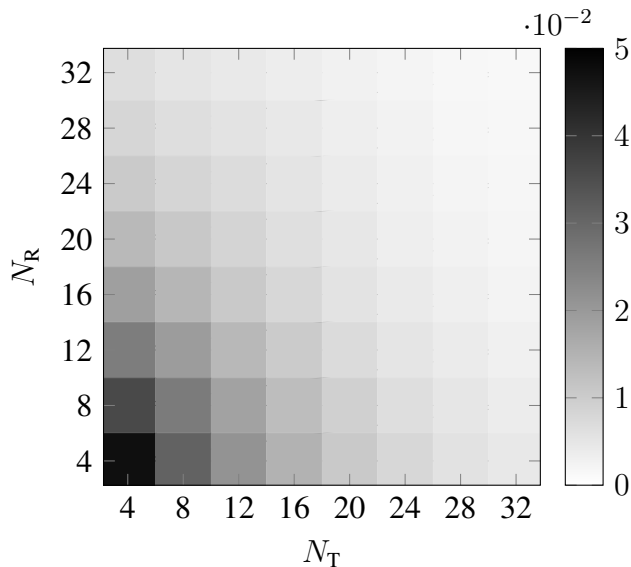


Fig. 3. Relative error of the asymptotic SPEB as a function of the number of transmit and receive antennas for different minimum angular separations.

position of the reflectors at $\mathbf{p}_{s,1} = [10 \text{ m}, 0 \text{ m}]^T$ and $\mathbf{p}_{s,1} = [-8 \text{ m}, 12 \text{ m}]^T$ and move the receiver in a $60 \text{ m} \times 60 \text{ m}$ area with the transmitter at its center, i.e. $-30 \text{ m} \leq p_{R,x} \leq 30 \text{ m}$, $-30 \text{ m} \leq p_{R,y} \leq 30 \text{ m}$. In Fig. 4 we plot the asymptotic PEB for a receiver with perfect KTT (Fig. 4(a)), with imperfect KTT, namely with $\sigma_{\text{clk}} = 0.5T_s \approx 2 \text{ ns}$ (Fig. 4(b)), and without KTT (Fig. 4(c)). Sub-meter positioning accuracy is attainable for all considered receiver locations, when perfect KTT or imperfect KTT with $\sigma_{\text{clk}} = 0.5T_s$ is available. However, when no KTT is available, there is significant accuracy degradation, because the positioning information from the LOS is no longer sufficient and information from the much weaker NLOS paths is required to compute the position. We observe that with imperfect KTT the PEB depends on the distance from the transmitter and the reflectors, whereas with perfect KTT it depends mainly on the distance from the transmitter. Also, we can see that clock synchronization errors with standard deviation as small as 2 ns can severely degrade the achievable positioning accuracy, compared to the case with perfect KTT.

C. The effect of Doppler shifts

To observe the effect of the Doppler shifts on the achievable positioning accuracy, we consider the setup used in the preceding numerical evaluations, but the receiver is now moving with

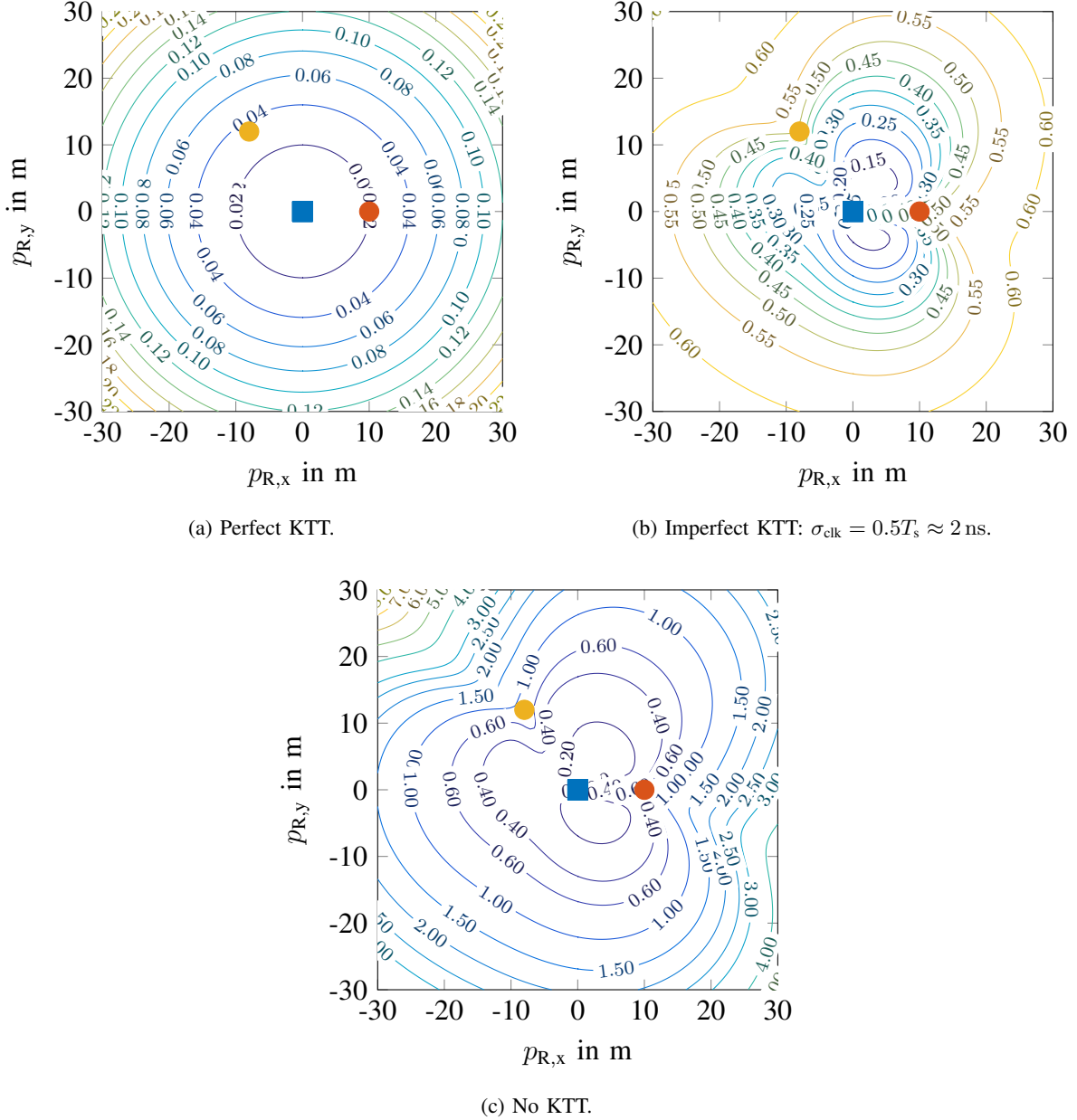


Fig. 4. PEB for receiver localization with $\mathbf{p}_T = [0 \text{ m}, 0 \text{ m}]^T$, $\mathbf{p}_{s,1} = [10 \text{ m}, 0 \text{ m}]^T$ and $\mathbf{p}_{s,2} = [-8 \text{ m}, 12 \text{ m}]^T$ under different levels of KTT. The position of the transmitter is shown with a square and the position of the reflectors with a circle.

velocity $\mathbf{v} = \mathbf{u}(\pi/4)150 \text{ km h}^{-1}$. Instead of 1 OFDM block, we now transmit $N_B = 32$ OFDM blocks, with a CP duration of $72T_s$, such that the synthetic array aperture is comparable to the physical aperture of the antenna arrays. We keep the total transmit power the same as in the static scenario, i.e. $N_B P_T = 20 \text{ dBm}$, so as to observe the effect of the receiver's movement for the same estimation SNR. We can see in Fig. 5 that, compared to the static case, the PEB

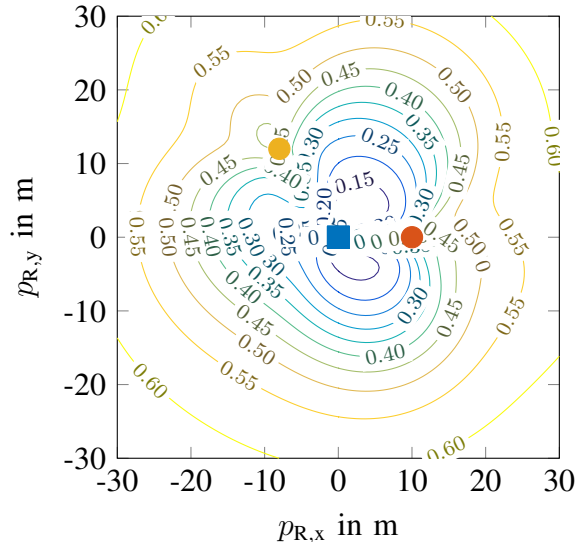
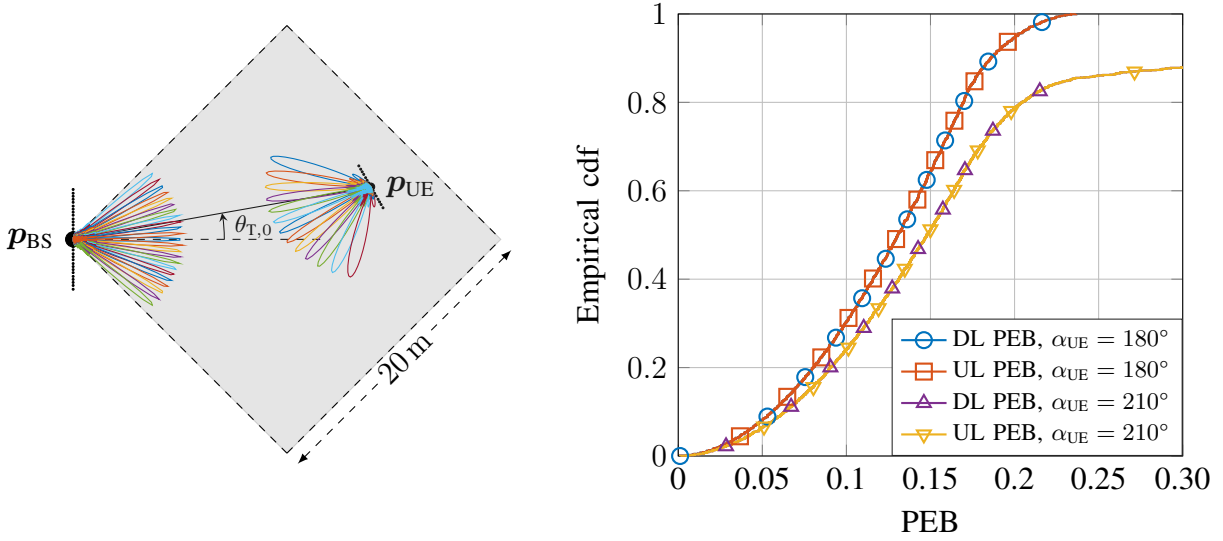


Fig. 5. PEB for receiver localization with $\mathbf{p}_T = [0 \text{ m}, 0 \text{ m}]^T$, $\mathbf{p}_{s,1} = [10 \text{ m}, 0 \text{ m}]^T$ and $\mathbf{p}_{s,2} = [-8 \text{ m}, 12 \text{ m}]^T$, receiver velocity $\mathbf{v} = \mathbf{u}(\pi/4)150 \text{ km h}^{-1}$, $\sigma_{\text{clk}} = 0.5T_s \approx 2 \text{ ns}$. The position of the transmitter is shown with a square and the position of the reflectors with a circle.

is improved (i.e. lower), especially for larger Tx-Rx distances, due to the angular information provided by the Doppler.

D. Downlink and Uplink Comparison

In our asymptotic analysis, where the transmitter and receiver can probe their entire transmit and receive spaces, we have found that downlink and uplink positioning are equivalent up to a scalar, which is equal to the ratio of the DL and UL SNR, and that the arrays' orientation affects the DL and UL in the same way. We now compare the DL and UL when only a part of the transmit and receive space can be excited, through a fixed set of beams. In a practical mm-Wave communication system this might be enforced by hardware constraints, e.g. when the number of RF chains is smaller than the number of antennas. We consider a static scenario and place the receiver in a square sector (90°), with edge length 20 m and the transmitter at one of its corners, as shown in Fig. 6(a). We consider LOS-only propagation and perfect KTT. The BS and the UE are equipped with ULAs. We set $N_{\text{BS}} = 32$ and $M_{\text{BS}} = 23$, which is equal to M_T in the DL and M_R in the UL. Similarly, we set $N_{\text{UE}} = 16$ and $M_{\text{UE}} = 13$, which is equal to M_R in the DL and M_T in the UL. The transmit (DL) and receive (UL) beams of the BS are chosen as the appropriate subset of the N_{BS} -sized DFT beams [34], to cover all possible UE locations in the given sector. Thus,



(a) Setup for comparison with the UE randomly placed in the square sector and $\alpha_{UE} = 210^\circ$. (b) PEB cdf for DL and UL positioning for different UE orientations.

Fig. 6. DL and UL positioning comparison with precoding and receive combining.

$[\mathbf{P}^{(DL)}]_{:,j} = [1, e^{-j\frac{2\pi}{N_{BS}}(j-(M_{BS}-1)/2)}, \dots, e^{-j\frac{2\pi}{N_{BS}}(N_{BS}-1)(j-(M_{BS}-1)/2)}]_{\text{T}} = \left([\mathbf{W}^{(UL)}]_{j,:}\right)^{\text{T}}, j = 0, \dots, M_{BS} - 1$. Similarly, the transmit (UL) and receive (DL) beams of the UE are $[\mathbf{P}^{(UL)}]_{:,i} = [1, e^{-j\frac{2\pi}{N_{UE}}(i-(M_{UE}-1)/2)}, \dots, e^{-j\frac{2\pi}{N_{UE}}(N_{UE}-1)(i-(M_{UE}-1)/2)}]_{\text{T}} = \left([\mathbf{W}^{(DL)}]_{i,:}\right)^{\text{T}}, i = 0, \dots, M_{UE} - 1$.

In both cases the available transmit power is uniformly allocated to the beams and the subcarriers, i.e. $\sum_{b=0}^{N_B-1} \mathbf{s}_b[p] \mathbf{s}_b^{\text{H}}[p] = N_B P_{\text{T}} / (N_{\text{T}} |\mathcal{P}|)$. The described setup is depicted in Fig. 6(a). Motivated by our findings about the relation between DL and UL positioning in Sec. V, but with M_{BS} and M_{UE} playing the role of N_{BS} and N_{UE} , we set $\sigma_{\eta,UE}^2 = 2\sigma_{\eta,BS}^2$ and $P_{UE} = P_{BS} \frac{\sigma_{\eta,BS}^2 M_{UE}}{\sigma_{\eta,UE}^2 M_{BS}}$, with $N_B P_{BS} = 20 \text{ dBm}$ and the noise spectral density of the BS $N_{0,BS} = -170 \text{ dBm Hz}^{-1}$. In Fig. 6(b), using the expressions for the exact CRLB from Sec. III, we plot the cumulative distribution function (cdf) for the PEB in the DL and UL for UE orientation 180° and 210° . We can observe that, for a given UE orientation, DL and UL positioning are equivalent under the same receive SNR, as in the case without precoding/receive combining. In general, the link with the highest receive SNR will provide the best performance, which is equal to the ratio of $P_{BS} M_{UE} / \sigma_{\eta,UE}^2$ and $P_{UE} M_{BS} / \sigma_{\eta,BS}^2$. The same result is also obtained when the BS and the UE use any set of orthogonal beams for transmission/reception. In addition, in contrast to [17], constraining the UE (and the BS) to transmit (UL) and receive (DL) through the same set of beams, we find that the orientation not only affects the UL, but also the DL positioning accuracy,

and in fact, it affects them in the same way. In the DL, due to the 210° UE orientation, for some UE locations the AOA of the LOS path is outside the range covered by the UE receive beams. Similarly, in the UL, for some UE locations the AOD of the LOS path is outside the range covered by the UE transmit beams.

VIII. CONCLUSION

We derived the exact and asymptotic expressions for the position, orientation and velocity error bounds for transmitter and receiver localization, in static and dynamic scenarios. We numerically verified a good convergence of the asymptotic to the exact bounds even for a moderate number of transmit and receive antennas. In addition, we analytically studied the impact of the quality of KTT on the derived bounds. By evaluating the bounds for different levels of KTT, we concluded that even small synchronization errors can significantly degrade the achievable positioning accuracy. Also, we provided numerical examples showing that mobility can in fact be exploited to improve the PEB. Furthermore, we used the bounds for transmitter and receiver localization to obtain an analytic relation between DL and UL positioning, showing that they differ only by a scalar. Finally, we numerically verified that a similar relation holds between UL and DL positioning even with fixed beamformers.

APPENDIX A

DERIVATIVES OF $\mathbf{m}_b[p]$ W.R.T. THE PARAMETERS IN THE CHANNEL PARAMETER VECTOR

In the following, we compute the partial derivatives of the $\mathbf{m}_b[p]$ w.r.t. the parameters in the channel parameter vector, which are used for the computation of the FIM of the channel parameter vector. We provide the required derivatives for the dynamic scenario; the required derivatives for the static scenario can be obtained from them by setting $\mathbf{v} = \mathbf{0}$ (or equivalently $v_l = 0, \forall l$), bearing in mind that $\lim_{v_l \rightarrow 0} Q(\tilde{\Phi}_{0,0,l}) = 1$ and $\lim_{v_l \rightarrow 0} Q(\tilde{\Phi}_{p,q,l}) = 0, p \neq q$, where $\tilde{\Phi}_{p,q,l} = (\omega_p - \omega_q - (\omega_c + \omega_q) v_l/c) T_s/2$. Setting $\tilde{\Psi}_{q,l,b} = \omega_q (\Delta\tau_l + \tau_s) - \frac{\omega_c + \omega_q}{c} v_l b M T_s$, we compute the required derivatives as

$$\frac{\partial \mathbf{m}_b[p]}{\partial \tau_s} = -j \sum_{q \in \mathcal{P}} \omega_q g[q] \sum_{l=0}^{L-1} h_l e^{-j \tilde{\Psi}_{q,l,b}} Q(\tilde{\Phi}_{p,q,l}) \mathbf{W} \mathbf{a}_{R,q}(\tilde{\theta}_{R,l}) \mathbf{a}_{T,q}^T(\tilde{\theta}_{T,l}) \mathbf{x}_b[q], \quad (41)$$

$$\frac{\partial \mathbf{m}_b[p]}{\partial \Delta\tau_l} = -j \sum_{q \in \mathcal{P}} \omega_q g[q] h_l e^{-j \tilde{\Psi}_{q,l,b}} Q(\tilde{\Phi}_{p,q,l}) \mathbf{W} \mathbf{a}_{R,q}(\tilde{\theta}_{R,l}) \mathbf{a}_{T,q}^T(\tilde{\theta}_{T,l}) \mathbf{x}_b[q], \quad (42)$$

$$\frac{\partial \mathbf{m}_b[p]}{\partial \theta_{T,l}} = \sum_{q \in \mathcal{P}} g[q] h_l e^{-j \tilde{\Psi}_{q,l,b}} Q(\tilde{\Phi}_{p,q,l}) \mathbf{W} \mathbf{a}_{R,q}(\tilde{\theta}_{R,l}) \mathbf{a}_{T,q}^T(\tilde{\theta}_{T,l}) \mathbf{D}_{T,q}(\tilde{\theta}_{T,l}) \mathbf{x}_b[q], \quad (43)$$

$$\frac{\partial \mathbf{m}_b[p]}{\partial \theta_{R,l}} = \sum_{q \in \mathcal{P}} g[q] h_l e^{-j \tilde{\Psi}_{q,l,b}} Q \left(\tilde{\Phi}_{p,q,l} \right) \mathbf{W} \mathbf{D}_{R,q} \left(\tilde{\theta}_{R,l} \right) \mathbf{a}_{R,q} \left(\tilde{\theta}_{R,l} \right) \mathbf{a}_{T,q}^T \left(\tilde{\theta}_{T,l} \right) \mathbf{x}_b [q], \quad (44)$$

$$\frac{\partial \mathbf{m}_b[p]}{\partial v_l} = \sum_{q \in \mathcal{P}} g[q] h_l e^{-j \tilde{\Psi}_{q,l,b}} Q \left(\tilde{\Phi}_{p,q,l} \right) V_{b,p,q,l} \mathbf{W} \mathbf{a}_{R,q} \left(\tilde{\theta}_{R,l} \right) \mathbf{a}_{T,q}^T \left(\tilde{\theta}_{T,l} \right) \mathbf{x}_b [q] \quad (45)$$

$$\frac{\partial \mathbf{m}_b[p]}{\partial h_{l,\Re}} = \sum_{q \in \mathcal{P}} g[q] e^{-j \tilde{\Psi}_{q,l,b}} Q \left(\tilde{\Phi}_{p,q,l} \right) \mathbf{W} \mathbf{a}_{R,q} \left(\tilde{\theta}_{R,l} \right) \mathbf{a}_{T,q}^T \left(\tilde{\theta}_{T,l} \right) \mathbf{x}_b [q], \quad (46)$$

$$\frac{\partial \mathbf{m}_b[p]}{\partial h_{l,\Im}} = j \frac{\partial \mathbf{m}_b[p]}{\partial h_{l,\Re}} \quad (47)$$

where $\mathbf{D}_{T,q} \left(\tilde{\theta}_{T,l} \right)$ is a diagonal matrix with $\left[\mathbf{D}_{T,q} \left(\tilde{\theta}_{T,l} \right) \right]_{j,j} = -j \frac{\omega_c + \omega_q}{c} d_{T,j} \mathbf{u}_\perp^T \left(\tilde{\theta}_{T,l} \right) \mathbf{u}(\psi_{T,j})$.

$$V_{b,p,q,l} = \left(\cot \left(\tilde{\Phi}_{p,q,l} \right) - N \cot \left(N \tilde{\Phi}_{p,q,l} \right) \right) T_s / 2 + j (bM + (N - 1) / 2) T_s. \quad (48)$$

APPENDIX B

ENTRIES OF FISHER INFORMATION TRANSFORMATION MATRICES

Here we list the derivatives of the parameters of the channel parameter vector ϕ w.r.t. the parameters of the position parameter vector $\tilde{\phi}$, which constitute the entries of the transformation matrices \mathbf{T}_R and \mathbf{T}_T . The entries of \mathbf{T}_T (\mathbf{T}_R) corresponding to identical parameters in ϕ and $\tilde{\phi}_T$ ($\tilde{\phi}_R$) are equal to 1, e.g. $\partial \tau_s / \partial \tau_s = 1$. Setting $d_{T,R} = \|\mathbf{p}_R - \mathbf{p}_T\|_2$, $d_{T,s,l} = \|\mathbf{p}_{s,l} - \mathbf{p}_T\|_2$ and $d_{R,s,l} = \|\mathbf{p}_R - \mathbf{p}_{s,l}\|_2$ the rest non-zero entries are computed as follows:

$$\frac{\partial \Delta \tau_l}{\partial \mathbf{p}_R} = \frac{\mathbf{u}(\theta_{R,0}) - \mathbf{u}(\theta_{R,l})}{c}, \quad (49) \quad \frac{\partial \Delta \tau_l}{\partial \mathbf{p}_T} = \frac{\mathbf{u}(\theta_{T,0}) - \mathbf{u}(\theta_{T,l})}{c}, \quad (53)$$

$$\frac{\partial \tilde{\theta}_{T,l}}{\partial \mathbf{p}_R} = \begin{cases} \frac{\mathbf{u}_\perp(\theta_{R,l})}{d_{T,R}}, & l = 0, \\ \mathbf{0}, & l \neq 0, \end{cases} \quad (50) \quad \frac{\partial \tilde{\theta}_{T,l}}{\partial \mathbf{p}_T} = \mathbf{u}_\perp(\theta_{T,l}) \begin{cases} \frac{1}{d_{T,R}}, & l = 0, \\ \frac{1}{d_{T,s,l}}, & l \neq 0, \end{cases} \quad (54)$$

$$\frac{\partial \tilde{\theta}_{R,l}}{\partial \mathbf{p}_R} = \mathbf{u}_\perp(\theta_{R,l}) \begin{cases} \frac{1}{d_{T,R}}, & l = 0, \\ \frac{1}{d_{R,s,l}}, & l \neq 0, \end{cases} \quad (51) \quad \frac{\partial \tilde{\theta}_{R,l}}{\partial \mathbf{p}_T} = \begin{cases} \frac{\mathbf{u}_\perp(\theta_{T,l})}{d_{T,R}}, & l = 0, \\ \mathbf{0}, & l \neq 0, \end{cases} \quad (55)$$

$$\frac{\partial \tilde{\theta}_{R,l}}{\partial \alpha_R} = -1, \quad (52) \quad \frac{\partial \tilde{\theta}_{T,l}}{\partial \alpha_T} = -1, \quad (56)$$

$$\frac{\partial \Delta \tau_l}{\partial \mathbf{p}_{s,l}} = \frac{\mathbf{u}(\theta_{T,l}) + \mathbf{u}(\theta_{R,l})}{c}, \quad (57)$$

$$\frac{\partial \tilde{\theta}_{T,l}}{\partial \mathbf{p}_{s,l}} = -\frac{\mathbf{u}_\perp(\theta_{T,l})}{d_{T,s,l}}, \quad (58)$$

$$\frac{\partial \tilde{\theta}_{R,l}}{\partial \mathbf{p}_{s,l}} = -\frac{\mathbf{u}_\perp(\theta_{R,l})}{d_{R,s,l}}. \quad (59)$$

With a mobile receiver

$$\frac{\partial v_l}{\partial \mathbf{p}_R} = -\rho_l \mathbf{u}_\perp(\theta_{R,l}) \begin{cases} \frac{1}{d_{T,R}}, & l = 0, \\ \frac{1}{d_{R,s,l}}, & l \neq 0, \end{cases} \quad (60)$$

$$\frac{\partial v_l}{\partial \mathbf{v}} = \mathbf{u}(\theta_{R,l}), \quad (61)$$

$$\frac{\partial v_l}{\partial \mathbf{p}_{s,l}} = \frac{\rho_l}{d_{R,s,l}} \mathbf{u}_\perp(\theta_{R,l}), \quad (62)$$

where $\rho_l = \mathbf{v}^T \mathbf{u}_\perp(\theta_{R,l})$. With a mobile transmitter

$$\frac{\partial v_l}{\partial \mathbf{p}_T} = -\rho_l \mathbf{u}_\perp(\theta_{T,l}) \begin{cases} \frac{1}{d_{T,R}}, & l = 0, \\ \frac{1}{d_{T,s,l}}, & l \neq 0, \end{cases} \quad (63)$$

$$\frac{\partial v_l}{\partial \mathbf{v}} = \mathbf{u}(\theta_{T,l}), \quad (64)$$

$$\frac{\partial v_l}{\partial \mathbf{p}_{s,l}} = \frac{\rho_l}{d_{T,s,l}} \mathbf{u}_\perp(\theta_{T,l}), \quad (65)$$

where $\rho_l = \mathbf{v}^T \mathbf{u}_\perp(\theta_{T,l})$.

APPENDIX C

PROOF OF THEOREM 1

We first have to compute the asymptotic expressions for the entries of the channel parameters FIM \mathbf{J}_ϕ , making use of the favorable propagation conditions and

$$\begin{aligned} \mathbf{a}_{T,p}^T(\tilde{\theta}_{T,l}) \mathbf{D}_{T,p}(\tilde{\theta}_{T,l}) \mathbf{a}_{T,p}^*(\tilde{\theta}_{T,l}) &= -j \frac{\omega_c + \omega_p}{c} \mathbf{u}_\perp^T(\tilde{\theta}_{T,l}) \sum_{j=1}^{N_T} d_{T,j} \mathbf{u}(\psi_{T,j}) \\ &= j \frac{\omega_c + \omega_p}{c} \mathbf{u}_\perp^T(\tilde{\theta}_{T,l}) N_T (\mathbf{p}_T - \bar{\mathbf{p}}_T) = 0, \end{aligned} \quad (66)$$

as we have chosen \mathbf{p}_T to be equal to the centroid of the array $\bar{\mathbf{p}}_T$. Similar expressions hold for the receiver. Also, in order to facilitate readability and understanding, instead of referring to the entries of \mathbf{J}_ϕ by their position in the matrix (i.e. number of row and column), we refer to them

by using as indices the variables they correspond to; for example, instead of $[\mathbf{J}_\phi]_{1,2}$ we write $J_{\tau_s \tilde{\theta}_{T,l}}$. Using the expressions above and the assumptions of Sec. IV, we find that

$$J_{\tau_s \tau_s} \rightarrow \delta_{R,T} \sum_{p \in \mathcal{P}} \gamma_p \omega_p^2 \sum_{l=0}^{L-1} |h_l|^2, \quad (67)$$

$$J_{\Delta \tau_l \Delta \tau_l} = J_{\tau_s \Delta \tau_l} \rightarrow \delta_{R,T} \sum_{p \in \mathcal{P}} \gamma_p \omega_p^2 |h_l|^2, \quad (68)$$

$$J_{\tilde{\theta}_{T,l} \tilde{\theta}_{T,l}} \rightarrow \delta_{R,T} |h_l|^2 \left(\frac{\bar{\omega}_c}{c} \right)^2 S_T \left(\tilde{\theta}_{T,l} \right), \quad (69)$$

$$J_{\tilde{\theta}_{R,l} \tilde{\theta}_{R,l}} \rightarrow \delta_{R,T} |h_l|^2 \left(\frac{\bar{\omega}_c}{c} \right)^2 S_R \left(\tilde{\theta}_{R,l} \right), \quad (70)$$

$$J_{h_l, \Re h_l, \Re} = J_{h_l, \Im h_l, \Im} \rightarrow \delta_{R,T}, \quad (71)$$

where with some abuse of notation the equality sign is used to denote that the asymptotic values are equal. We also compute $J_{\tau_s h_l, \Re} = J_{\Delta \tau_l h_l, \Re} \rightarrow \delta_{R,T} h_l, \Im \sum_{p \in \mathcal{P}} \gamma_p \omega_p$ and $J_{\tau_s h_l, \Im} = J_{\Delta \tau_l h_l, \Im} \rightarrow -\delta_{R,T} h_l, \Re \sum_{p \in \mathcal{P}} \gamma_p \omega_p$. The rest entries of the FIM are (exactly or asymptotically) zero. We can see that the information about the channel gains is only coupled with the information about the time-related parameters $\tau_s, \{\Delta \tau_l\}_{l=0}^{L-1}$. Using the notion of the EFIM, we can show that in terms of position and orientation information it is equivalent to consider parameter vectors not including the channel gains, but include the uncertainty they introduce to the model by replacing the time-related FIM entries $J_{\tau_s \tau_s}, \{J_{\Delta \tau_l \Delta \tau_l}, J_{\tau_s \Delta \tau_l}\}_{l=0}^{L-1}$ with $J'_{\tau_s \tau_s}, \{J'_{\Delta \tau_l \Delta \tau_l}, J'_{\tau_s \Delta \tau_l}\}_{l=0}^{L-1}$, where

$$J'_{\tau_s \tau_s} \rightarrow \delta_{R,T} \beta^2 \sum_{l=0}^{L-1} |h_l|^2, \quad (72)$$

$$J'_{\Delta \tau_l \Delta \tau_l} = J'_{\tau_s \Delta \tau_l} \rightarrow \delta_{R,T} \beta^2 |h_l|^2. \quad (73)$$

The only term requiring further attention is $J_{\tilde{\theta}_{T,l} \tilde{\theta}_{R,l'}}$ for $l \neq l'$, as for $l = l'$ it is $J_{\tilde{\theta}_{T,l} \tilde{\theta}_{R,l}} = 0$ due to (66). Using the favorable propagation conditions and the asymptotic expressions derived above we can find that as $F_s, N_T, N_R \rightarrow \infty$, these entries become negligible compared to the other non-zero entries of \mathbf{J}_ϕ . Thus, they can be ignored in the following computation of the asymptotic position and orientation EFIM. In the following, in order to make the expressions more compact, when the same variable is used in both indices we write it only once; e.g. we write J_{τ_s} instead of $J_{\tau_s \tau_s}$. We then compute

$$\mathbf{T}_{\text{po}} \mathbf{J}_\phi \mathbf{T}_{\text{po}}^T = \frac{J_{\tilde{\theta}_{T,0}}}{d_{T,R}^2} \mathbf{z}_{\theta_{T,0}} \mathbf{z}_{\theta_{T,0}}^T + \frac{J_{\tilde{\theta}_{R,0}}}{d_{T,R}^2} \mathbf{z}_{\theta_{R,0}} \mathbf{z}_{\theta_{R,0}}^T + \sum_{l=1}^{L-1} \left(\frac{J'_{\Delta \tau_l}}{c^2} \mathbf{z}_{l,t} \mathbf{z}_{l,t}^T + \frac{J_{\tilde{\theta}_{R,l}}}{d_{R,s,l}^2} \mathbf{z}_{l,a} \mathbf{z}_{l,a}^T \right) \quad (74)$$

where $\mathbf{z}_{l,t} = [\mathbf{u}^\top(\theta_{R,0}) - \mathbf{u}^\top(\theta_{R,l}) \quad 0]^\top$ and $\mathbf{z}_{l,a} = [\mathbf{u}_\perp^\top(\theta_{R,l}) \quad -d_{R,s,l}]^\top$. We also write

$$\mathbf{T}_{np} \mathbf{J}_\phi \mathbf{T}_{np}^\top = \begin{bmatrix} J'_{\tau_s} & \mathbf{b}^\top \\ \mathbf{b} & \mathbf{C} \end{bmatrix}, \quad (75)$$

where $\mathbf{b} = [J'_{\Delta\tau_1} (\mathbf{u}(\theta_{T,1}) + \mathbf{u}(\theta_{R,1}))^\top / c, \dots, J'_{\Delta\tau_{L-1}} (\mathbf{u}(\theta_{T,L-1}) + \mathbf{u}(\theta_{R,L-1}))^\top / c]^\top$ and \mathbf{C} is a block diagonal matrix with the following 2×2 matrices at its diagonal:

$$\begin{aligned} \mathbf{J}_{s,l} &= \frac{J'_{\Delta\tau_l}}{c^2} (\mathbf{u}(\theta_{T,l}) + \mathbf{u}(\theta_{R,l})) (\mathbf{u}(\theta_{T,l}) + \mathbf{u}(\theta_{R,l}))^\top + \frac{J_{\tilde{\theta}_{T,l}}}{d_{T,s,l}^2} \mathbf{u}_\perp(\theta_{T,l}) \mathbf{u}_\perp^\top(\theta_{T,l}) \\ &\quad + \frac{J_{\tilde{\theta}_{R,l}}}{d_{R,s,l}^2} \mathbf{u}_\perp(\theta_{R,l}) \mathbf{u}_\perp^\top(\theta_{R,l}). \end{aligned} \quad (76)$$

In order to compute $(\mathbf{T}_{np} \mathbf{J}_\phi \mathbf{T}_{np}^\top)^{-1}$ using block matrix inversion, we still need to compute \mathbf{C}^{-1} , which in turn, using block diagonal matrix inversion, requires the computation of $\mathbf{J}_{s,l}^{-1}$. We compute $\mathbf{J}_{s,l}^{-1}$ as [12, Lemma 1]

$$\begin{aligned} \mathbf{J}_{s,l}^{-1} &= \frac{1}{|\mathbf{J}_{s,l}|} \left[\frac{J'_{\Delta\tau_l}}{c^2} (\mathbf{u}_\perp(\theta_{T,l}) + \mathbf{u}_\perp(\theta_{R,l})) (\mathbf{u}_\perp(\theta_{T,l}) + \mathbf{u}_\perp(\theta_{R,l}))^\top \right. \\ &\quad \left. + \frac{J_{\tilde{\theta}_{T,l}}}{d_{T,s,l}^2} \mathbf{u}(\theta_{T,l}) \mathbf{u}^\top(\theta_{T,l}) + \frac{J_{\tilde{\theta}_{R,l}}}{d_{R,s,l}^2} \mathbf{u}(\theta_{R,l}) \mathbf{u}^\top(\theta_{R,l}) \right], \end{aligned} \quad (77)$$

with

$$|\mathbf{J}_{s,l}| = \frac{J'_{\Delta\tau_l}}{c^2} (1 + \cos(\Delta\theta_l))^2 \left(\frac{J_{\tilde{\theta}_{T,l}}}{d_{T,s,l}^2} + \frac{J_{\tilde{\theta}_{R,l}}}{d_{R,s,l}^2} \right) + \frac{J_{\tilde{\theta}_{T,l}} J_{\tilde{\theta}_{R,l}}}{d_{T,s,l}^2 d_{R,s,l}^2} \sin^2(\Delta\theta_l). \quad (78)$$

Therefore, using these, $\mathbf{u}^\top(\theta_{T,l}) \mathbf{u}(\theta_{R,l}) = \cos(\Delta\theta_l)$ and $\mathbf{u}^\top(\theta_{T,l}) \mathbf{u}_\perp(\theta_{R,l}) = \sin(\Delta\theta_l)$, after some algebraic manipulations we find that

$$\begin{aligned} &\mathbf{T}_{po} \mathbf{J}_\phi \mathbf{T}_{np}^\top (\mathbf{T}_{np} \mathbf{J}_\phi \mathbf{T}_{np}^\top)^{-1} \mathbf{T}_{np} \mathbf{J}_\phi \mathbf{T}_{po}^\top \\ &= \sum_{l=1}^{L-1} \left[\frac{(J'_{\Delta\tau_l})^2}{c^4} \frac{(1 + \cos(\Delta\theta_l))^2}{|\mathbf{J}_{s,l}|} \left(\frac{J_{\tilde{\theta}_{T,l}}}{d_{T,s,l}^2} + \frac{J_{\tilde{\theta}_{R,l}}}{d_{R,s,l}^2} \right) \mathbf{z}_{l,t} \mathbf{z}_{l,t}^\top \right. \\ &\quad \left. + \frac{J_{\tilde{\theta}_{R,l}}^2}{d_{R,s,l}^4} \left(\frac{J'_{\Delta\tau_l}}{c^2} \frac{(1 + \cos(\Delta\theta_l))^2}{|\mathbf{J}_{s,l}|} + \frac{J_{\tilde{\theta}_{T,l}} \sin^2(\Delta\theta_l)}{d_{T,s,l}^2 |\mathbf{J}_{s,l}|} \right) \mathbf{z}_{l,a} \mathbf{z}_{l,a}^\top \right. \\ &\quad \left. + \frac{J'_{\Delta\tau_l} J_{\tilde{\theta}_{T,l}} J_{\tilde{\theta}_{R,l}} (1 + \cos(\Delta\theta_l)) \sin(\Delta\theta_l)}{c^2 d_{T,s,l}^2 d_{R,s,l}^2 |\mathbf{J}_{s,l}|} (\mathbf{z}_{l,t} \mathbf{z}_{l,a}^\top + \mathbf{z}_{l,a} \mathbf{z}_{l,t}^\top) \right] + \frac{1}{\hat{K}_{\tau_s}} \hat{\mathbf{z}}_{\tau_s} \hat{\mathbf{z}}_{\tau_s}^\top \end{aligned} \quad (79)$$

where

$$\begin{aligned} \hat{K}_{\tau_s} &= \frac{J'_{\tau_s} - \sum_{l=1}^{L-1} J'_{\Delta\tau_l}}{c^2} + \sum_{l=1}^{L-1} \left[\frac{J'_{\Delta\tau_l} J_{\tilde{\theta}_{T,l}} J_{\tilde{\theta}_{R,l}}}{c^2 d_{T,s,l}^2 d_{R,s,l}^2 |\mathbf{J}_{s,l}|} \sin^2(\Delta\theta_l) \right] \\ \hat{\mathbf{z}}_{\tau_s} &= \sum_{l=1}^{L-1} \frac{J'_{\Delta\tau_l} J_{\tilde{\theta}_{T,l}} J_{\tilde{\theta}_{R,l}}}{c^2 d_{T,s,l}^2 d_{R,s,l}^2 |\mathbf{J}_{s,l}|} \sin(\Delta\theta_l) \mathbf{z}_l \end{aligned}$$

Combining (74) and (79) we find that the position and orientation EFIM is

$$\mathbf{J}_{\text{po}} \rightarrow \frac{J_{\tilde{\theta}_{T,0}}}{d_{T,R}^2} \mathbf{z}_{\theta_{T,0}} \mathbf{z}_{\theta_{T,0}}^T + \frac{J_{\tilde{\theta}_{R,0}}}{d_{T,R}^2} \mathbf{z}_{\theta_{R,0}} \mathbf{z}_{\theta_{R,0}}^T + \sum_{l=1}^{L-1} \frac{J'_{\Delta\tau_l} J_{\tilde{\theta}_{T,l}} J_{\tilde{\theta}_{R,l}}}{c^2 d_{T,s,l}^2 d_{R,s,l}^2 |\mathbf{J}_{s,l}|} \mathbf{z}_l \mathbf{z}_l^T - \frac{1}{\hat{K}_{\tau_s}} \hat{\mathbf{z}}_{\tau_s} \hat{\mathbf{z}}_{\tau_s}^T. \quad (80)$$

Finally, using (80) and (69)-(73) we obtain the desired result.

REFERENCES

- [1] A. Dammann, R. Raulefs, and S. Zhang, "On prospects of positioning in 5G," in *Proc. IEEE Int. Conf. Commun. Workshop (ICCW)*, London, UK, Jun. 2015, pp. 1207–1213.
- [2] K. Witrisal *et al.*, "High-accuracy localization for assisted living: 5G systems will turn multipath channels from foe to friend," *IEEE Signal Process. Mag.*, vol. 33, no. 2, pp. 59–70, Mar. 2016.
- [3] K. Witrisal, S. Hinteregger, J. Kulmer, E. Leitinger, and P. Meissner, "High-accuracy positioning for indoor applications: RFID, UWB, 5G, and beyond," in *Proc. IEEE 10th Int. Conf. RFID (RFID)*, Orlando, FL, May 2016, pp. 1–7.
- [4] H. Wymeersch, G. Seco-Granados, G. Destino, D. Dardari, and F. Tufvesson, "5G mmWave positioning for vehicular networks," *IEEE Wireless Commun.*, vol. 24, no. 6, pp. 80–86, Dec. 2017.
- [5] A. Kakkavas, M. H. Castañeda Garcia, R. A. Stirling-Gallacher, and J. A. Nossek, "Multi-array 5G V2V relative positioning: Performance bounds," in *Proc. IEEE Global Commun. Conf. (GLOBECOM)*, Abu Dhabi, United Arab Emirates, Dec. 2018, to be published.
- [6] A. Hakkarainen, J. Werner, M. Costa, K. Leppanen, and M. Valkama, "High-efficiency device localization in 5G ultra-dense networks: Prospects and enabling technologies," in *Proc. IEEE 82th Veh. Technol. Conf. (VTC-Fall)*, Boston, MA, Sep. 2015, pp. 1–5.
- [7] P. Kela, M. Costa, J. Turkka, M. Koivisto, J. Werner, A. Hakkarainen, M. Valkama, R. Jantti, and K. Leppanen, "Location based beamforming in 5G ultra-dense networks," in *2016 IEEE 84th Vehicular Technology Conference (VTC-Fall)*, Sep. 2016, pp. 1–7.
- [8] F. Maschietti, D. Gesbert, P. de Kerret, and H. Wymeersch, "Robust location-aided beam alignment in millimeter wave massive mimo," in *Proc. IEEE Global Commun. Conf. (GLOBECOM)*, Singapore, Dec. 2017, pp. 1–6.
- [9] Y. Shen and M. Z. Win, "Fundamental limits of wideband localization - part I: A general framework," *IEEE Trans. Inf. Theory*, vol. 56, no. 10, pp. 4956–4980, Oct. 2010.
- [10] Y. Shen, H. Wymeersch, and M. Z. Win, "Fundamental limits of wideband localization - part II: Cooperative networks," *IEEE Trans. Inf. Theory*, vol. 56, no. 10, pp. 4981–5000, Oct. 2010.
- [11] Y. Shen and M. Z. Win, "Fundamental limits of wideband localization accuracy via Fisher information," in *Proc. IEEE Wireless Commun. Netw. Conf. (WCNC)*, Kowloon, Hong Kong, Mar. 2007, pp. 3046–3051.
- [12] —, "On the use of multipath geometry for wideband cooperative localization," in *Proc. IEEE Global Commun. Conf. (GLOBECOM)*, Honolulu, HI, USA, Nov. 2009, pp. 1–6.
- [13] Y. Han, Y. Shen, X. P. Zhang, M. Z. Win, and H. Meng, "Performance limits and geometric properties of array localization," *IEEE Trans. Inf. Theory*, vol. 62, no. 2, pp. 1054–1075, Feb. 2016.
- [14] A. Guerra, F. Guidi, and D. Dardari, "Position and orientation error bound for wideband massive antenna arrays," in *Proc. IEEE Int. Conf. Commun. Workshop (ICCW)*, London, UK, Jun. 2015, pp. 853–858.
- [15] —, "Single anchor localization and orientation performance limits using massive arrays: MIMO vs. beamforming," *ArXiv e-prints*, Feb. 2017.

- [16] A. Shahmansoori, G. E. Garcia, G. Destino, G. Seco-Granados, and H. Wymeersch, "5G position and orientation estimation through millimeter wave MIMO," in *Proc. IEEE Globecom Workshops (GC Wkshps)*, San Diego, CA, Dec. 2015, pp. 1–6.
- [17] Z. Abu-Shaban, X. Zhou, T. Abhayapala, G. Seco-Granados, and H. Wymeersch, "Error bounds for uplink and downlink 3D localization in 5G mmWave systems," *IEEE Trans. Wireless Commun.*, 2018.
- [18] R. Mendrzik, H. Wymeersch, G. Bauch, and Z. Abu-Shaban, "Harnessing NLOS components for position and orientation estimation in 5G mmwave MIMO," *ArXiv e-prints*, Dec. 2017.
- [19] A. Shahmansoori, G. E. Garcia, G. Destino, G. Seco-Granados, and H. Wymeersch, "Position and orientation estimation through millimeter-wave MIMO in 5G systems," *IEEE Trans. Wireless Commun.*, vol. 17, no. 3, pp. 1822–1835, Mar. 2018.
- [20] J. Talvitie, M. Valkama, G. Destino, and H. Wymeersch, "Novel algorithms for high-accuracy joint position and orientation estimation in 5G mmWave systems," in *Proc. IEEE Globecom Workshops (GC Wkshps)*, Singapore, Dec. 2017, pp. 1–7.
- [21] R. Mendrzik, H. Wymeersch, and G. Bauch, "Joint localization and mapping through millimeter wave MIMO in 5G systems - extended version," *ArXiv e-prints*, Apr. 2018.
- [22] Z. Abu-Shaban, H. Wymeersch, T. Abhayapala, and G. Seco-Granados, "Single-anchor two-way localization bounds for 5G mmWave systems: Two protocols," *ArXiv e-prints*, May 2018.
- [23] R. Vaughan and J. Bach-Anderson, *Channels, propagation and antennas for mobile communications*, ser. IEE electromagnetic waves series. Stevenage: The Institution of Engineering and Technology, 2003.
- [24] T. S. Rappaport, E. Ben-Dor, J. N. Murdock, and Y. Qiao, "38 Ghz and 60 Ghz angle-dependent propagation for cellular & peer-to-peer wireless communications," in *Proc. IEEE Int. Conf. Commun. (ICC)*, Ottawa, Canada, Jun. 2012, pp. 4568–4573.
- [25] M. T. Martinez-Ingles, D. P. Gaillot, J. Pascual-Garcia, J. M. Molina-Garcia-Pardo, M. Lienard, and J. V. Rodriguez, "Deterministic and experimental indoor mmW channel modeling," *IEEE Antennas Wireless Propag. Lett.*, vol. 13, pp. 1047–1050, 2014.
- [26] M. Peter *et al.*, "Measurement campaigns and initial channel models for preferred suitable frequency ranges; Deliverable D2.1," Mar. 2016. [Online]. Available: <https://5g-mmmagic.eu/results/#deliverables>
- [27] K. Gröchenig, *Foundations of Time-Frequency Analysis*, ser. Applied and Numerical Harmonic Analysis. Birkhäuser Boston, 2001.
- [28] T. Rappaport, *Wireless Communications: Principles and Practice*, 2nd ed. Upper Saddle River, NJ, USA: Prentice Hall PTR, 2001.
- [29] S. M. Kay, *Fundamentals of Statistical Signal Processing: Estimation Theory*. Upper Saddle River, NJ, USA: Prentice-Hall, Inc., 1993.
- [30] E. L. Lehmann and G. Casella, *Theory of Point Estimation (Springer Texts in Statistics)*, 2nd ed. Springer New York, Aug. 1998.
- [31] J. Chen, "When does asymptotic orthogonality exist for very large arrays?" in *Proc. IEEE Global Commun. Conf. (GLOBECOM)*, Atlanta, GA, USA, Dec. 2013, pp. 4146–4150.
- [32] H. Q. Ngo, E. G. Larsson, and T. L. Marzetta, "Aspects of favorable propagation in massive MIMO," in *22nd European Signal Processing Conference (EUSIPCO)*, Lisbon, Portugal, Sep. 2014, pp. 76–80.
- [33] C. Masouros and M. Matthaiou, "Space-constrained massive MIMO: Hitting the wall of favorable propagation," *IEEE Commun. Lett.*, vol. 19, no. 5, pp. 771–774, May 2015.
- [34] G. H. Song, J. Brady, and A. Sayeed, "Beamspace MIMO transceivers for low-complexity and near-optimal communication at mm-wave frequencies," in *Proc. IEEE Int. Conf. Acoust., Speech and Signal Process. (ICASSP)*, Vancouver, BC, Canada, May 2013, pp. 4394–4398.